Water Resources Research

RESEARCH ARTICLE
10.1029/2024WR038954

Special Collection:
Integrating In Situ, Remote Sensing, And Physically Based Modeling Approaches to Understand Global Freshwater Ice Dynamics

Long-Term Lake Ice Evolution in a Large Endorheic Lake Undergoing Accelerated Shrinkage in a Semiarid Region of China

Tingfeng Wu[1], Anning Huang[2], Qi Zhang[1], Justin Brookes[3], Wenming Yan[1], Boqiang Qin[4], Dequan Han[5], and Xiaofei Hu[4]

[1]National Key Laboratory of Water Disaster Prevention, Yangtze Institute for Conservation and Development, Hohai University, Nanjing, China, [2]School of Atmospheric Sciences, Nanjing University, Nanjing, China, [3]School of Biological Science, University of Adelaide, Adelaide, SA, Australia, [4]Nanjing Institute of Geography and Limnology, Chinese Academy of Sciences, Nanjing, China, [5]Ulanqab Hydrology and Water Resources Subcenter, Ulanqab, China

Abstract Long-term lake ice evolution under climate change has attracted global attention. However, despite the widespread occurrence of lake shrinkage in endorheic regions worldwide, few studies have explicitly addressed its effects on lake ice regimes. This study fills this research gap by investigating the long-term evolution of lake ice in Lake Daihai—a large shrinking endorheic lake in China—by integrating six decades (1960–2022) of hydrometeorological data, retrieved Landsat images, and experiments with a three-dimensional hydrodynamics-ice numerical model. Our results show that Lake Daihai experienced accelerated shrinkage at an average rate of −2.18 km^2 yr^{-1} from 1960 to 2022, which was primarily driven by intensified anthropogenic activities and increased evaporation. Concurrently, the annual average lake ice thickness exhibited an accelerated decreasing trend at an average rate of −0.39 cm yr^{-1}. This ice-thinning trend was attributed to the processes of atmospheric warming (air temperature increase: 2.5°C), salinization (increase in salinity: 451.3%), and morphological changes associated with lake shrinkage (water depth reduction: −12 m; surface area reduction: −72.9%). Model experiments reveal3ed that the representative factors (i.e., air temperature, salinity, and average water depth) of these processes were significantly correlated with ice phenology metrics (i.e., ice-on date, ice-off date, and ice duration); their relative contributions to ice thinning were 36.1%, 18.9%, and −15.2%, respectively, and the wind speed contributed 3.5%. Ice thinning was driven mainly by atmospheric warming but slowed by lake shrinkage characterized by a decrease in the average water depth. Under ongoing global warming, ice-thinning is projected to accelerate by 2031 because of the nonlinear increase in the contribution of salinization in this shrinking lake. These findings highlight that traditional climate-centric models may underestimate or overestimate lake ice dynamics if they fail to account for salinization or morphological changes, underscoring the necessity of developing integrated assessment frameworks tailored to shrinking endorheic lakes.

Key Points:

- Lake Daihai underwent accelerated shrinkage, salinization and ice thinning from 1960 to 2022
- Air temperature, salinity, wind speed, and average water depth affected ice phenology and contributed to ice thinning by 36.1%, 18.9%, 3.5%, and −15.2%, respectively
- Shrinkage and salinization are projected to intensify future ice evolution, highlighting their critical roles in improving climate–ice models

Correspondence to:
T. Wu, Q. Zhang, W. Yan, and B. Qin,
WUTINGFENG@hhu.edu.cn;
qizhang@hhu.edu.cn;
ywm0815@hhu.edu.cn;
qinbq@niglas.ac.cn

Citation:
Wu, T., Huang, A., Zhang, Q., Brookes, J., Yan, W., Qin, B., et al. (2025). Long-term lake ice evolution in a large endorheic lake undergoing accelerated shrinkage in a semiarid region of China. *Water Resources Research*, *61*, e2024WR038954. https://doi.org/10.1029/2024WR038954

Received 24 SEP 2024
Accepted 4 DEC 2025

Author Contributions:
Conceptualization: Tingfeng Wu, Anning Huang, Qi Zhang, Justin Brookes, Boqiang Qin
Data curation: Tingfeng Wu, Anning Huang, Wenming Yan, Dequan Han, Xiaofei Hu
Formal analysis: Tingfeng Wu, Anning Huang, Qi Zhang, Justin Brookes, Wenming Yan, Xiaofei Hu
Funding acquisition: Qi Zhang, Boqiang Qin

1. Introduction

Lakes cover approximately 2% of Earth's terrestrial surface (Brown & Duguay, 2010). These freshwater systems provide a wide range of ecosystem services, including fish harvest, cultural practices, transportation, recreation, and regulation of the hydrological cycle (Arp et al., 2019; Farmer et al., 2015; Li et al., 2024; Sharma et al., 2023; Wang, Song, et al., 2018). Notably, lacustrine ecosystems in cryospheric environments (alpine/arctic latitudes >55°N) experience seasonal ice cover that lasts 4–9 months each year (Sharma et al., 2023). This cryolacustrine interface has sparked significant scientific research on ice phenology, ice thermodynamics, and ice-mediated ecological constraints (Hampton et al., 2017; Leppäranta, 2023; Woolway et al., 2020; Woolway & Merchant, 2019).

The formation of lake ice is dictated by surface energy balance dynamics and emerges through complex interactions among atmospheric forcing (thermal and mechanical), lacustrine geometry, and hydrological factors (Woolway et al., 2020). Lake ice phenology (ice-on, ice duration, and ice-off) serves as a sensitive climate proxy (Kirillin et al., 2012; Woolway et al., 2020). Therefore, numerous studies have sought to quantify the long-term trends in lake ice phenology in response to meteorological factors related to climatic warming (Grant et al., 2021; Huang et al., 2022; Magnuson et al., 2000; Walsh et al., 1998). However, less attention has been given to

Investigation: Tingfeng Wu, Dequan Han, Xiaofei Hu
Methodology: Tingfeng Wu, Anning Huang
Project administration: Boqiang Qin
Resources: Tingfeng Wu, Anning Huang, Qi Zhang, Dequan Han
Software: Tingfeng Wu, Xiaofei Hu
Supervision: Qi Zhang, Boqiang Qin
Validation: Tingfeng Wu, Anning Huang, Justin Brookes, Wenming Yan, Dequan Han
Visualization: Tingfeng Wu, Anning Huang, Wenming Yan, Xiaofei Hu
Writing – original draft: Tingfeng Wu
Writing – review & editing: Anning Huang, Qi Zhang, Justin Brookes, Boqiang Qin

understanding the contributions of other factors, such as lake morphology (Brown & Duguay, 2010; Kirillin et al., 2012; Sharma et al., 2020).

Lake morphology (lake geometry ratio, lake area, and lake depth) influences lake ice phenology through its effects on wind fetch patterns, water circulation dynamics, thermal regimes, and heat content (Jeffries & Morris, 2007; Magee & Wu, 2017; Rafat et al., 2023; Smits et al., 2021; Williams et al., 2004). Compared with shallower lakes, deeper lakes with higher heat contents experience more frequent ice-free winters, later freeze onset dates, earlier thaw timing, and consequently shorter ice-covered periods (Bernhardt et al., 2012; Blagrave & Sharma, 2023; Martynov et al., 2010). However, conflicting evidence exists, with some studies reporting minimal impacts of the lake morphology on ice phenological patterns (Smits et al., 2021; Williams & Stefan, 2006). This disparity highlights the current lack of a scientific consensus regarding the relative importance of morphological metrics in regulating lake ice dynamics.

The current understanding of lake morphology–ice phenology relationships predominantly stems from cross-lake comparative analyses (Brown & Duguay, 2011; Robertson et al., 1992; Sharma et al., 2019), leaving a critical knowledge gap regarding the effects of intralake morphology on long-term trends in lake ice phenology in a single lake. Prevailing assumptions suggest that natural lakes exhibit minimal morphological shifts over decadal scales compared with climatic changes, thereby rendering morphological metrics negligible in driving observed ice phenology trends (Gebre et al., 2014; Hodgkins et al., 2002; Patterson & Swindles, 2015). This conclusion, however, emerges from methodologically constrained investigations that primarily employ one-dimensional modeling frameworks under idealized conditions (Bernhardt et al., 2012; Brown & Duguay, 2010; Dibike et al., 2011; Gebre et al., 2014; Magee & Wu, 2017). Such simplified models inherently fail to capture the spatial heterogeneity in ice formation processes (Wu, Huang, et al., 2023). Consequently, their ability to quantify morphological controls on ice phenology trajectories remains fundamentally limited.

Accumulating evidence has revealed significant morphological transformations in global lakes since the 1980s (Pekel et al., 2016), particularly through expansion/shrinkage dynamics in arid and semiarid regions (Su et al., 2023; Tao et al., 2015; Wang, Song, et al., 2018; Woolway et al., 2020). These transformations necessitate an explicit consideration of their potential impacts on ice phenological cycles. Neglecting these morphodynamical processes may lead to a biased attribution of the observed ice regime changes solely to climate change.

Advanced hydrodynamic modeling technology now enable sophisticated three-dimensional hydrodynamic-ice simulation (Anderson et al., 2018; Wu, Huang, et al., 2023; Ye et al., 2019), and overcome the spatial limitations of traditional one-dimensional approaches. This methodological advancement provides an opportunity to disentangle climate–morphology interactions in long-term ice evolution.

Lakes across the Mongolian Plateau, which mirror the global trend of lake changes in arid and semiarid regions, have undergone accelerated shrinkage in recent decades (Tao et al., 2015; Wang, Song, et al., 2018). As a critical case study, Lake Daihai is the third largest endorheic lake in the Inner Mongolian Autonomous Region of China. It has undergone particularly rapid changes, including lake shrinkage, salinization and ice-thinning. Although considerable attention has been given to the role of lake ice in supporting the ecosystem services of Lake Daihai (Hou et al., 2024; Yang et al., 2024), no studies have yet examined the long-term evolution of lake ice in this shrinking endorheic lake. Consequently, the drivers of lake ice dynamics remain poorly understood. This study investigated the evolution of lake ice in Lake Daihai from 1960 to 2022, with the following objectives:

1. To clarify six decades of lake shrinkage and ice evolution patterns in Lake Daihai;
2. To quantify the relative contributions of morphological changes (lake area and lake depth), salinization, and atmospheric forcing to lake ice evolution.

Through the integration of ground observations, retrieved Landsat images, and numerical modeling experiments, we systematically disentangle the mechanistic interactions between thermal forcing components, hydrochemical shifts, and bathymetric modifications.

2. Data and Methods

2.1. Study Area

Lake Daihai (40°32′ to 40°37′N, 112°37′ to 112°46′E) is a representative endorheic lake system located in the mid-temperate semiarid zone of China in the Mongolian Plateau ecoregion (Figure 1a), on which most lakes have

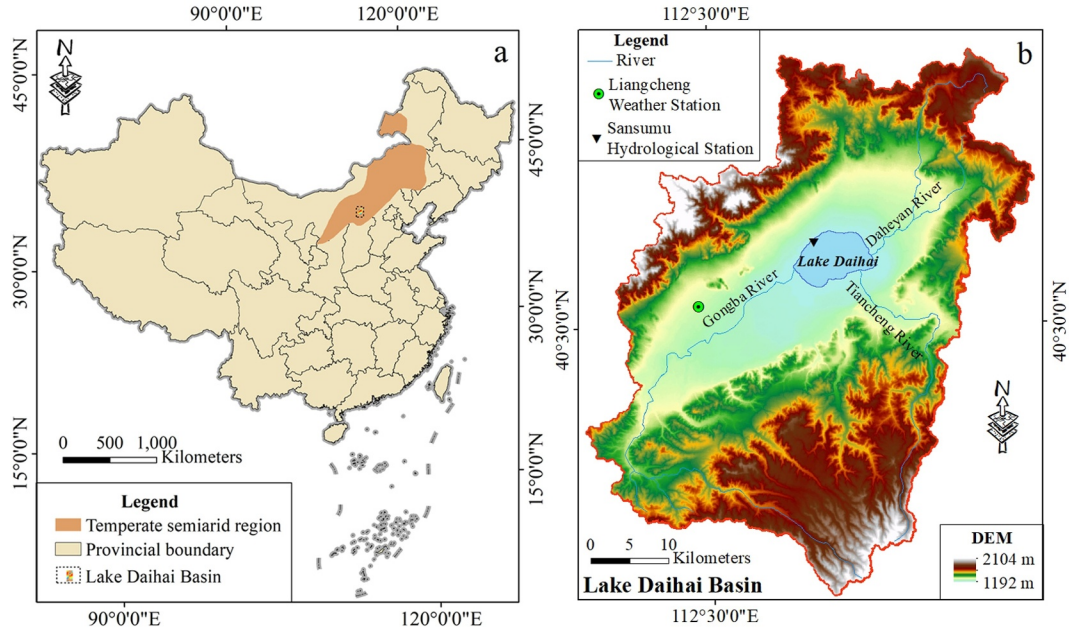

Figure 1. (a) Geographical setting of the Lake Daihai Basin within the mid-temperate semiarid zone of China; (b) basin topography, perennial/ephemeral tributary networks, Lake Daihai, and locations of the Liangcheng Weather Station and Sansumu Hydrological Station.

experienced shrinkage (Tao et al., 2015). This lake is a hydrologically closed basin, encompassing 2,341.7 km^2 (Figure 1b), and has undergone continuous shrinkage (Wu, Liu, et al., 2023). In the early 1960s, it had an area of 177.5 km^2 (Yang et al., 2022) and a water storage value of 135 $\times 10^8$ m^3. However, the lake area had decreased by 71% in 2019.

The water balance of Lake Daihai demonstrates critical seasonality: the Gongba River experiences seasonal freezing, the Tiancheng and Daheyan Rivers completely desiccate during cold periods (Ren et al., 2022). This hydrological regime effectively decouples the lake from fluvial inputs throughout the winter half-year (November–April; Chun et al., 2020; Wang et al., 2022), creating closed-system dynamics prior to 2022.

The Lake Daihai Basin, which is located in a representative agro-pastoral zone of northern China, is characterized by a mid-temperate semiarid monsoonal continental climate with long, cold winters and short, warm summers (Ren et al., 2022; Wang et al., 2022). The annual maximum, mean, and minimum air temperatures are 39.3°C, 5.2°C, and −34.5°C, respectively. The annual total precipitation (410 mm) is distributed unevenly throughout the year, and the annual total evaporation is 983.6 mm. The precipitation from June to September (flood season) accounts for 76.7% of the annual precipitation. The annual mean sunshine hours are approximately 3,000 hr, and the annual wind speed is approximately 2.3 m s^{-1}, with the predominant wind directions being west and northwest.

Snowfall in the Lake Daihai Basin primarily occurs from the preceding November to the following April, with an average monthly snow depth of 34 mm from 1960 to 2022. Similarly, the lake ice phenological cycle of Lake Daihai typically begins with freeze initiation in early December (or late November) of the preceding year, reaches the maximum ice thickness in February, and completely melts by late April. The average monthly ice thickness was 0.47 ± 0.15 m. However, this natural rhythm has been disrupted since 2005 because of thermal effluent discharge from the adjacent Daihai power plant (Chun et al., 2020; Figure 10 in Section 3.2.1). Notably, such thermal effluent discharge was prohibited in 2019. Wu, Liu, et al. (2023) measured the lake ice thickness at seven uniformly distributed sampling points across the lake on a single day in January 2021. They observed that the lake ice thickness ranged from 34 to 46.5 cm on that day, indicating significant spatial variability in the lake ice thickness with this lake. As detailed in Section 3.1.3, the lake ice thickness decreased significantly. Lake ice thinning resulted in suspensions of the Winter Fishing Festival, water plant closure (Huang et al., 1997; Zhang

et al., 2020), intensified eutrophication (Hou et al., 2024; Li et al., 2024; Meng et al., 2023; Wu, Liu, et al., 2023), and increased greenhouse gas emissions (Yang et al., 2024).

2.2. Data

The hourly air temperature, wind speed and direction, surface pressure, relative humidity, precipitation, sunshine hours, and evaporation data from 1960 to 2022 were collected from Liangcheng Weather Station, which is located 14 km southwest of Lake Daihai and has a 0.5% elevation difference (Figure 1b). Complementary radiative components (cloud cover, surface downward solar radiation, and surface downward thermal radiation) were retrieved from the ERA5-Land reanalysis data set (0.1° spatial resolution; ECMWF Copernicus Climate Data Store, https://cds.climate.copernicus.eu/). This multimodal data set integrates in situ measurements with gridded atmospheric modeling outputs, ensuring temporal continuity (hourly) and spatial consistency across the 63-year observation period.

Hydrological monitoring of Daihai Lake was conducted at the Sansumu Hydrological Station (Figure 1b), with daily measurements of the water level referenced to the Yellow Sea Datum recorded continuously from 1960 to 2022 at 8:00 local solar time. The Sansumu Hydrological Station is one of the national hydrological stations of the Ministry of Water Resources of the People's Republic of China. All monitoring activities comply with the nationally unified standards. Ice thickness monitoring during the winter half-year followed a 5-day interval protocol throughout the 63-year observation period. Ice thickness was measured at a specific ice monitoring site (40°35′N, 112°39′E), which can represent the annual ice dynamics in Lake Daihai. Water temperature was measured at a 0.2 m depth during the summer months at a time interval of 10 days from 1960 to 1991 and 1 day after 1991. Lake bathymetry data from 2004 were provided by the Hydrological Survey Bureau of Ulanqab city, Inner Mongolia Autonomous Region, China. The salinity data compilation integrated directly measured values in intermittent periods (1962–1963, 1971, 1974, 1984–1990, 1992, 1994–1996, 2003–2004, 2009, 2015–2021) sourced from published studies (Figure 6a; Chun et al., 2020; Yang et al., 2023), with estimated values in other years derived through regression equations.

Satellite-derived lacustrine boundaries and Lake Daihai ice data were obtained from Landsat TM/ETM+/OLI data sets (30 m spatial resolution, <5% cloud cover) via the USGS/NASA Earth Explorer platform (http://earthexplorer.usgs.gov) spanning 1986–2021. A total of 239 cloud-free Landsat scenes were acquired and processed. These multispectral images underwent radiometric calibration and geometric rectification using toolkits in ENVI/SNAP software to enable the precise extraction of lacustrine boundaries and ice-covered areas. The temporal scope was constrained by the absence of pre-1986 Landsat archival records for this inland basin. Furthermore, complementary bathymetric reconstruction employed Advanced Spaceborne Thermal Emission and Reflection Radiometer Global Digital Elevation Model (ASTER GDEM) data acquired on 9 June 2004 (https://worldview.earthdata.nasa.gov/). This 30-m resolution elevation product facilitated historical shoreline reconstruction corresponding to the 1961 hydrological baseline. In addition, Sentinel-2 satellite images (10 m spatial resolution, <5% cloud cover) were obtained and processed using the Google Earth Engine (GEE) platform (https://earthengine.google.com/).

2.3. Analytical Methods and Modeling

2.3.1. Retrieval of Lake Shoreline and Ice Data

The annual lake morphology was determined based on the lake shoreline configuration and bathymetric characteristics. The Normalized Difference Water Index (NDWI; McFeeters, 1996) was applied to systematically delineate the shoreline boundaries of Lake Daihai using cloud-free Landsat TM/ETM+/OLI images (1986–2022).

$$\mathrm{NDWI} = \frac{\mathrm{Green} - NIR}{\mathrm{Green} + NIR} \tag{1}$$

where Green and *NIR* represent the reflectance values of the green and near-infrared spectral bands, respectively. The shoreline boundaries were delineated using a threshold of 0.3 and were subsequently postprocessed through manual correction to limit geolocation errors to within a single pixel resolution of the image. Spectral bands corresponding to visible and near-infrared wavelengths (bands 1 (blue), 3 (red), and 4 (green) in the Landsat TM/

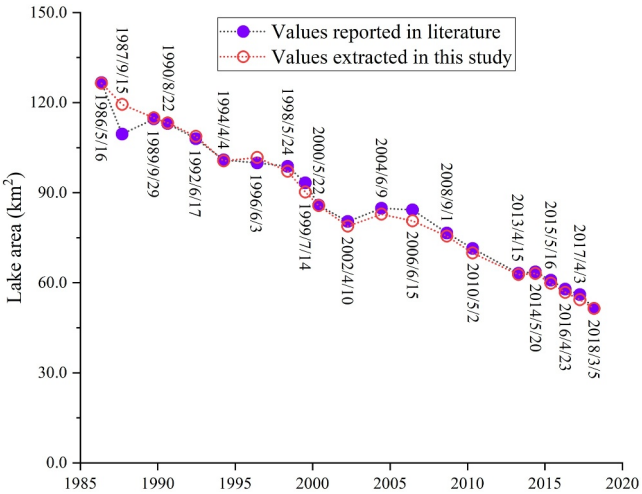

Figure 2. Comparisons between lake areas reported in the literature and those delineated from Landsat images in this study.

ETM + images from 1986 to 2012, and bands 2 (blue), 4 (red), and 5 (green) in the Landsat OLI images from 2013 to 2022 were utilized to delineate lake shorelines. In addition, parts of the images (Figure 10) were used to analyze the influences of thermal effluent discharge on the annual ice phenology dynamics in Lake Daihai.

Chen et al. (2020) documented the shoreline boundaries and lake area of Lake Daihai for 1986–2018, and these data were used to validate our shoreline extraction (Figure 2). The validation results showed a strong correlation between the lake area estimates from this study and those from the literature ($r = 0.99$, $p < 0.01$), with a root mean square error (RMSE) of 1.58 km^2. Moreover, the lake morphology delineated here aligns closely with the morphological patterns described by Chen et al. (2020) and Wang et al. (2022).

Since no precise shoreline maps or satellite imagery of Lake Daihai from the 1960s were available, the historical shoreline of 1961 was reconstructed by integrating the following data sources: (a) ASTER GDEM data acquired on 9 June 2004 (Figure 1b), (b) monthly water level records, (c) bathymetric surveys conducted in 2004, and (d) morphological parameters derived from Feng et al. (1994). Prior to reconstruction, the elevation values referenced to the Yellow Sea Datum were converted to mean sea level (MSL) to maintain consistency with the vertical reference framework of the ASTER GDEM.

Additionally, Sentinel-2 satellite images with high sampling frequency and resolution were used to validate the lake ice dynamics during the winter-half year of 2020–2021 simulated by the three-dimensional hydrodynamics–ice model described in Section 2.3.2. The reason for selecting 2020–2021 is that the Sentinel satellite images are available after 2017. All available Sentinel-2 satellite images during the winter half-year of 2020–2021 were downloaded and combined into a false color composite of bands 2 (blue), 4 (red), and 8 (near-infrared).

2.3.2. Lake Ice Model

Recent advances in lacustrine ice modeling have increased the adoption of three-dimensional hydrodynamic models for simulating ice dynamics (Oveisy et al., 2012; Wu, Huang, et al., 2023; Ye et al., 2019). Notably, the Finite Volume Community Ocean Model–Los Alamos Sea Ice Model (FVCOM-CICE; Gao et al., 2011) has been operationally integrated into the next-generation National Oceanic and Atmospheric Administration (NOAA) Great Lakes Operational Forecast System (GLOFS), demonstrating a robust ability to capture the interannual variability in ice across the Laurentian Great Lakes (Anderson et al., 2018). Building upon these advancements, we implemented the FVCOM-CICE model to investigate ice phenological dynamics in Lake Daihai. In addition, this model was originally developed for marine environments where salinity serves as an indispensable variable that regulates ice dynamics (Chen et al., 2012; Hunke et al., 2015).

2.3.2.1. Model Configurations

The FVCOM is a three-dimensional, unstructured, free-surface, primitive-equation, sigma-coordinate oceanographic model that solves the integral form of the governing equations. This model has been extensively validated in lacustrine environments and has shown robust performance across diverse hydrodynamic studies (Anderson et al., 2010; Morales-Marín et al., 2017; Nakada et al., 2021; Tang et al., 2020; Zhao et al., 2012).

Fujisaki-Manome et al. (2020) configured the FVCOM-CICE model for Lake Erie using unstructured triangular meshes with a horizontal resolution ranging from approximately 200 m near the shoreline to 2,500 m offshore. Based on their findings and preliminary comparative simulations of horizontal resolution, a resolution of approximately 400 m was adopted for lake ice simulations in Lake Daihai. This value is near the lower end of the horizontal resolution range used in their study, reflecting the considerably smaller size of Lake Daihai than Lake Erie. Our model utilizes 5 sigma layers to ensure an adequate vertical resolution, achieving a vertical resolution of approximately 1–3 m across most lake regions. This configuration is consistent with the vertical resolution of the model for Lake Erie, which employs 21 sigma layers and maintains a vertical resolution of less than 3 m.

Furthermore, the time step is set to 10 s for the external mode and 40 s for the internal mode, as constrained by the Courant–Friedrichs–Lewy condition.

Apart from the configuration of spatial and temporal discretization, horizontal diffusion is parameterized using the Smagorinsky scheme, while vertical diffusion is closured by a vertical mixing coefficient. The air–water drag coefficient is calculated as a function of the wind speed (LP1981; Large & Pond, 1981). Latent and sensible heat fluxes are calculated from the Coupled Ocean-Atmosphere Response Experiment (COARE) algorithm (Fairall et al., 2003).

The FVCOM-CICE model was first developed by coupling the FVCOM and CICE models (Gao et al., 2011), enabling high-resolution simulations of two-dimensional ice properties, including concentration, thickness distribution, and drift velocity. This coupled system has shown versatility across diverse lacustrine environments (Anderson et al., 2018; Bai et al., 2020; Fujisaki-Manome et al., 2020; Ye et al., 2019). The horizontal meshes and time step (40 s) of the CICE model are identical to those of the hydrodynamic model. The ice surface albedo is dynamically calculated as a function of the surface temperature, ice thickness, and visible and infrared spectral bands of incoming solar radiation (Briegleb et al., 2002; Ye et al., 2019). The net momentum and heat transfer are calculated as weighted averages of the air–water and ice–water stresses by the areal fraction of ice and weighted averages of the air–water and ice–water heat fluxes, respectively (Maykut & McPhee, 1995).

Model inputs and outputs: The input conditions of the FVCOM-CICE model consist of computational meshes (Figure 3), initial conditions (water temperature, flow, water level, and salinity), and boundary conditions (atmospheric forcing), each of which is described in detail below. The model outputs include water depth, three-dimensional flow velocity, water temperature, salinity, water density, ice concentration, ice thickness, ice surface temperature, snow thickness, and two-dimensional ice velocity in each mesh.

Simulation years and computational meshes: Given the absence of Landsat TM/ETM + images prior to 1985, shoreline data spanning 1986–2022 and the reconstructed historical shoreline of 1961 and future shoreline of 2031 (Section 3.1.1) were utilized to generate model computational meshes.

As noted above, several studies have reported minimal impacts of lake morphology on ice phenology (Smits et al., 2021; Williams & Stefan, 2006). One plausible explanation is that morphological changes in most lakes occur slowly. For instance, although Lake Daihai underwent accelerated shrinkage, its interannual shoreline variation was less than 5%. The year 1961 was selected as the control simulation year to illustrate the influence of lake morphology on ice regimes because the lake area in 1961 was substantially larger than that in the other years from 1986 to 2022 (Section 3.1.1). The simulation results from this year were then compared with those from other selected years, which were spaced at five-year intervals from 1986 to 2022. This sampling strategy was adopted for three primary reasons. (a) The FVCOM-CICE model cannot simulate the dynamics of wetting–drying zones, rendering it unsuitable for continuous multiyear simulations, particularly in lakes undergoing substantial morphological changes. This result could explain why the simulation duration of the FVCOM-CICE model is typically 1–2 years in numerous other lake ice modeling studies (Bai et al., 2020; Fujisaki-Manome et al., 2020; Ye et al., 2019). (b) Changes in lake morphology over 5-year intervals are more pronounced than those occurring annually. (c) Long-term measured data and simulations from the selected years are sufficient to elucidate the characteristics of the decrease in lake ice thickness in Lake Daihai and its influencing factors.

Accordingly, nine simulation years (1961, 1986, 1991, 1996, 2001, 2006, 2011, 2016, and 2021) and a forecast year (2031) were selected to simulate annual lake ice cycles from 1 October of the preceding year to 31 May (Table 1). The model simulation for a simulation year or the forecast year was initialized on 1 October of the preceding year and terminated on 31 May.

Ten computational meshes were generated by integrating the shoreline and bathymetric data for nine simulation years and one forecast year (Figure 3), using SMS software (Aquaveo LLC, USA). Notably, the shoreline of the forecast year was delineated based on the water level and lake area estimated from their respective decreasing rates during the third phase (Section 3.1.1) using ArcMap (ESRI Inc., USA).

Initial conditions: The water temperature was initialized as spatially uniform (15°C isothermal), and the flow velocity was set to 0 m s^{-1}. These uniform initial values may introduce considerable errors (i.e., spin-up effects). The simulation period began 2 months prior to winter to minimize the spin-up effects. This approach ensures that the model reaches equilibrium with atmospheric forcing and renders the freeze-up date insensitive to initialization

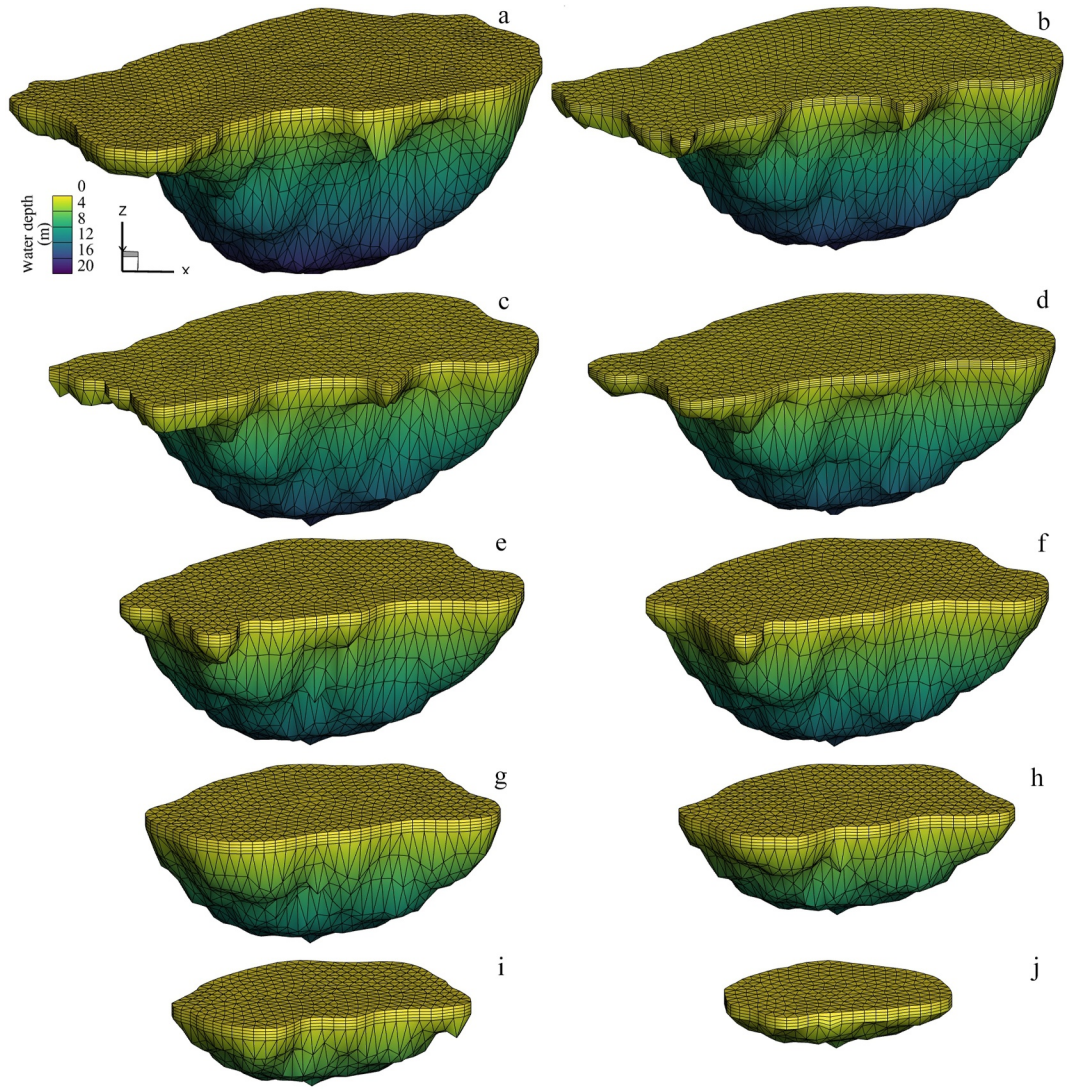

Figure 3. The three-dimensional underwater topography (i.e., lake morphology) and corresponding computational meshes of Lake Daihai utilized in the FVCOM-CICE model are shown for the following years: (a) 1961, (b) 1986, (c) 1991, (d) 1996, (e) 2001, (f) 2006, (g) 2011, (h) 2016, (i) 2021, and (j) 2031.

(Liston & Hall, 1995). Ice formation in Lake Daihai typically starts in early December or late November; hence, October 1st was selected as the simulation start time. Moreover, water turnover occurs in autumn months (September, October, and November) and leads to a more uniform vertical distribution of temperature, density, and salinity, which further helps reduce the spin-up effects. Additionally, the initial water level and annual salinity values were assigned based on the measured values corresponding to the start of each simulation year.

Boundary conditions: Atmospheric forcing (air temperature, wind speed, wind direction, surface pressure, precipitation, potential evaporation, surface downward solar radiation, surface downward thermal radiation, cloud cover, relative humidity, and specific humidity) was generated using MATLAB (MathWorks Inc., USA) and input into the FVCOM-CICE model. The salinity of the precipitation was set to 0‰. River inflow was excluded from the simulations, as all the rivers are frozen in this closed lake during the winter half-year (Wang et al., 2022). Additionally, thermal discharge from the Daihai power plant (2005–2019) was omitted because data were unavailable.

Notably, although the meshes and boundary conditions differ across these 10 simulation years, their initial conditions and parameter settings are identical.

Table 1
Lake Characteristics Across Simulation Years and Configurations of the Model Experiments

Year	Lake area (km^2)	Average water depth (m)	Salinity (‰)	Model experiments
1961	168.3	6.68	2.82	① Control experiments ② Morphology experiments ③ Salinity experiments ④ Air temperature experiments ⑤ Wind speed experiments ⑥ Forecast experiments
1986	128.2	6.69	4.14	
1991	112.3	6.26	5.19	
1996	100.7	6.4	5.72	
2001	83.4	6.43	6.16	
2006	80.8	6.44	6.56	
2011	67.8	5.64	7.23	
2016	56.5	4.4	8.32	
2021	48.3	3.28	13.09	
2031	30.8	1.57	18.19	

2.3.2.2. Model Calibration and Validation

The lake ice thickness measured at the lake ice observation site of Lake Daihai (Figure 1b) was used to calibrate and validate the FVCOM-CICE model. Specifically, measured lake ice thickness data from 1961 to 1986 were used for model calibration, whereas data from other simulation periods (1991 1996, 2001, 2006, 2011, 2016, and 2021) were used for model validation.

2.3.3. Model Experiments

Six model experiments were systematically designed to quantify the effects of morphology, salinity, air temperature, and wind speed on lake ice dynamics.

① *Control experiments* (control—1961, 1986, 1991, 1996, 2001, 2006, 2011, 2016, and 2021) were implemented to assess model performance (model calibration and validation). The FVCOM-CICE model was driven by the measured initiation and boundary conditions of each simulation year to simulate water temperature, ice area, and ice thickness, using the model configurations described above.

② *Morphology experiments* (morphology—1986, 1991 1996, 1999, 2001, 2006, 2011, 2016, and 2021) were designed to isolate the individual effects of changes in lake morphology on lake ice dynamics. These experiments replaced the lake morphology of the control—1961 with the lake morphology in 1986, 1991, 1996, 1999, 2001, 2006, 2011, 2016, and 2021 (nine meshes) and retained the remaining model configurations of the control—1961.

③ *Salinity experiments* (salinity—1986, 1991 1996, 1999, 2001, 2006, 2011, 2016, and 2021) were designed to elucidate the individual effects of changes in lake salinity on lake ice dynamics. These experiments replaced the salinity of the control—1961 with the salinity in 1986, 1991, 1996, 2001, 2006, 2011, 2016, and 2021 and retained remaining model configurations of the control—1961.

④ *Air temperature experiments* (air temperature—1986, 1991 1996, 1999, 2001, 2006, 2011, 2016, and 2021) were designed to elucidate the individual effects of changes in air temperature on lake ice dynamics. These experiments replaced the air temperature of the control—1961 with the air temperature of 1986, 1991, 1996, 1999, 2001, 2006, 2011, 2016, and 2021 and retained remaining model configurations of the control—1961.

⑤ *Wind speed experiments* (wind speed—1986, 1991 1996, 1999, 2001, 2006, 2011, 2016, and 2021) were designed to elucidate the individual effects of changes in wind speed on lake ice dynamics. These experiments replaced the wind speed of the control—1961 with the wind speed in 1986, 1991, 1996, 1999, 2001, 2006, 2011, 2016, and 2021 and retained remaining model configurations of the control—1961.

⑥ *Forecast experiments* (forecasted morphology—2031, forecasted salinity—2031, forecasted air temperature—2031, and forecasted all—2031) were designed to forecast lake ice dynamics from 1 October 2030 to 31 May 2031. Specifically, the forecasted values of lake morphology, air temperature, salinity, or all three forecasted metrics for 2031, which were derived from historical data, were used to replace the corresponding values of the control—1961. The remaining model configurations from the control-1961 were retained.

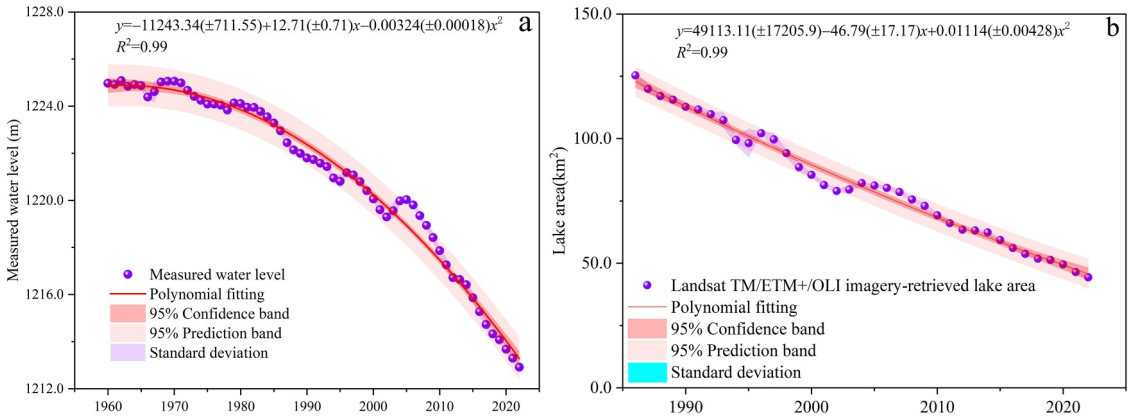

Figure 4. Variations in the annual average and standard deviation of the measured water level and Landsat TM/ETM+/OLI imagery-retrieved lake area from 1986 to 2022 and their polynomial fits.

2.4. Statistical Analysis

The winter half-year was quantified using day counting number in which the first day (November 1) was assigned a value of 1 and the last day (April 30) was assigned a value of 181 or 182. Lake-wide ice thickness was constrained to ≥5 cm during simulations because thinner ice covers are prone to destroy by hydrodynamic processes (Oveisy et al., 2012). Ice phenological metrics were defined as follows: the ice-on date corresponds to the first occurrence in winter when the average lake ice thickness exceeds 5 cm, the ice-off date corresponds to the first occurrence in spring when the average lake ice thickness decreases below 5 cm, and the ice duration represents the time interval between the ice-on date and the ice-off date.

The total lake heat content (H) was estimated by integrating the heat content of all the model meshes (Ye et al., 2019).

$$H = \sum_{i=1}^{n} \rho_i C_w V_i T_i \tag{2}$$

where V_i and T_i are the lake volume and water temperature in each mesh, respectively; C_w is the specific heat of water; and ρ_i is the water density in each mesh.

Lake ice model performance was evaluated using the root mean square error (RMSE), mean bias deviation (MBD), and mean bias (BIAS) (Bai et al., 2020; Magee & Wu, 2017; Oveisy et al., 2012; Wu, Huang, et al., 2023). Hydrometeorological metrics are presented as the means ± standard deviations and were calculated using Microsoft Excel (Microsoft Corp., USA). Pearson's correlation coefficients (R) between variables are reported at the significance levels of both $p < 0.05$ and $p < 0.01$. Regression analyses on the lake ice or hydrometeorological metrics from 1960 to 2021 were conducted to assess the changing trends of the time series. Both correlation and regression analyses were performed using IBM SPSS Statistics (IBM Corp., USA). Temporal changes in the vertical water temperature profile were visualized using Hovmöller diagrams (Hocke & Kämpfer, 2011).

3. Results

3.1. Lake Shrinkage and Ice Thickness Observations

3.1.1. Lake Shrinkage

Lake shrinkage is characterized by long-term decreases in lake morphological metrics (water level and lake area). A regression analysis of water level time series from the Sansumu Hydrological Station in China indicated a significant decrease from 1,225 ± 0.14 m in 1960 to 1,212.9 ± 0.1 m in 2022 ($p < 0.05$; Figure 4a). This decreasing process consists of three phases: a slow decrease of −5.68 cm yr^{-1} (1960–1978), a moderate decrease of −19.07 cm yr^{-1} (1979–2005), and a rapid decrease of −43.09 cm yr^{-1} (2006–2022). These trends are attributed

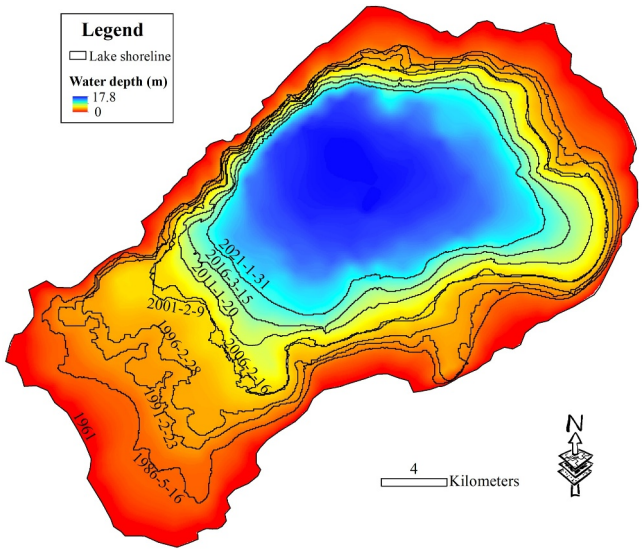

Figure 5. Water depth and ASTER GDEM data-rebuilt lake shoreline of 1961 and Landsat TM/ETM+/OLI imagery-retrieved lake shorelines from 1986, 1991, 1996, 2001, 2006, 2011, 2016, and 2021.

primarily to a combination of anthropogenic (local economic development) and climatic drivers (Chun et al., 2020; Wang et al., 2022). Despite the overall decreasing trend, episodic water level increases occurred during the 1960s, 1970s, 1990s, and 2000s. Additionally, the 63-year average monthly water level variability was minimal, with a maximum difference of 0.2 m.

The analyses of the available Landsat images (239 satellite scenes) revealed a marked reduction in the lake surface area from 125.38 ± 1.71 km^2 in1986 to 44.35 ± 0.67 km^2 in 2022, yielding an annual average recession rate of −2.14 km^2 yr^{-1} ($p < 0.05$; Figure 4b). The lake area in 2022 decreased by 79% relative to the lake area in 1961 (163.76 km^2). The most pronounced shoreline retreat occurred in the southwestern region of Lake Daihai because of the shallow bathymetry in this region (Figure 5). The lake area was strongly positively correlated with the water level ($R = 0.96$, $p < 0.01$) and exhibited a sustained multidecadal decline punctuated by episodic recovery phases. Additionally, the lake showed limited intra-annual variability, as evidenced by the constrained multiannual mean standard deviation (1.28 km^2) in the lake area.

3.1.2. Lake Water Salinity

As an endorheic lake without outflow, water loss from Lake Daihai occurs mainly through evaporation (Wang et al., 2022). Evaporation led to a substantial increase in salinity from 2.8‰ in 1960 to 13.09‰ in 2021 ($p < 0.05$; Figure 6a), with discernible phase-dependent acceleration (0.03‰ yr^{-1}, 0.12‰ yr^{-1}, and 0.51‰ yr^{-1}) corresponding to three successive phases of lake shrinkage. Notably, compared with the preceding decades, the post-2006 period experienced a 4.25-fold increase in salinity. This nonlinear acceleration has been mechanistically attributed to the increase in lake water temperature resulting from thermal effluent discharge from the Daihai Power Plant (Chun et al., 2020).

3.1.3. Lake Ice Thickness

As lake shrinkage and salinization progressed, the lake ice phenological cycles significantly varied over the 63-year observation period. The average value of the measured lake ice thickness in the winter half-year significantly decreased from 0.47 ± 0.15 m in 1960 to 0.26 ± 0.12 m in 2022, which is equivalent to an average reduction rate of −0.39 cm yr^{-1} (Figure 7a). Similarly, the maximum ice thickness markedly decreased from 0.63 m in 1960 to 0.41 m in 2022, which is equivalent to an average reduction rate of −0.42 cm yr^{-1}, while its occurrence date increased insignificantly (Figure 7b). The thinning of lake ice also displayed distinct temporal phases: a slow decrease of −0.003 m yr^{-1} (1960–1978), a moderate decrease of −0.0067 m yr^{-1} (1979–2005), and a rapid decrease of −0.0081 m yr^{-1} (2006–2022). Additionally, the rate of decrease in ice thickness varied by month from 1960 to 2022, with February (0.57 ± 0.11 m) showing the greatest reduction at −0.0047 m yr^{-1}, followed by March (−0.0042 m yr^{-1} for 0.49 ± 0.13 m), January (−0.0042 m yr^{-1} for 0.46 ± 0.1 m), and December (−0.003 m yr^{-1} for 0.24 ± 0.08 m). These results indicate that a significant ice-thinning process occurred in Lake Daihai over the 63-year observation period.

3.1.4. Meteorological Metrics

Atmospheric forcing was regarded as the primary driver of lake ice evolution, as supported by the multivariate mereological analysis using data from the Liangcheng Weather Station. The 63-year (1960–2022) average values of mereological metrics were as follows: air temperature, −6.8 ± 1.3°C; wind speed, 2.4 ± 0.5 m s^{-1}; pressure, 87,585.9 ± 79 pa; relative humidity, 51.5 ± 6%; precipitation, 4.9 ± 2.8 mm; sunshine hours, 220.9 ± 15.7 hr; and potential evaporation, −33.3 ± 4.1 mm. The average air temperature in the winter half-year significantly increased at a rate of 0.04°C yr^{-1} over the 63-year observation period ($p < 0.01$; Figure 6b), whereas wind speed and sunshine hours significantly decreased at rates of −0.01675 m yr^{-1} and −0.33361 hr yr^{-1}, respectively ($p < 0.01$; Figures 6c and 6d). Notably, these trends remained consistent across the three phases without evidence of acceleration. The remaining meteorological metrics (i.e., pressure, relative humidity, precipitation, and potential evaporation) did not change significantly over the 63-year observation period. In addition to these

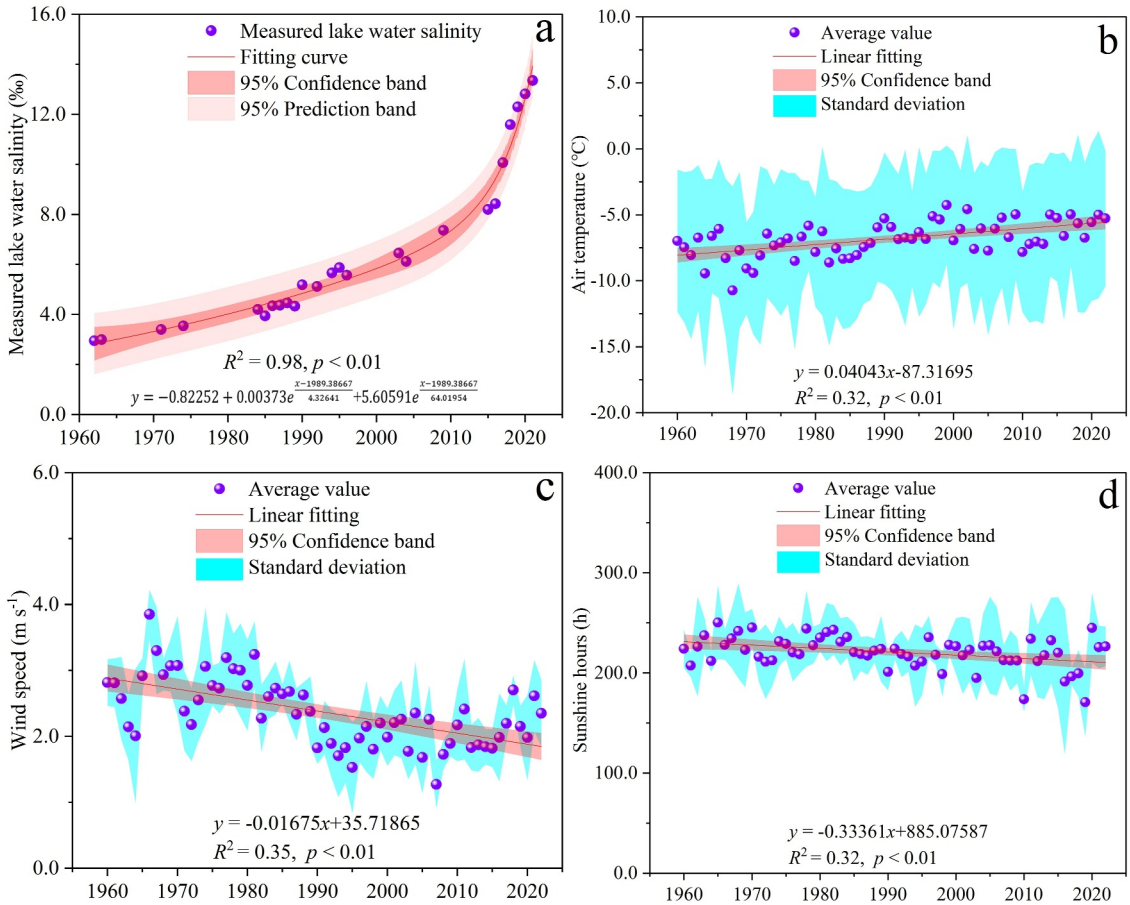

Figure 6. Variations in the average salinity (a), air temperature (b), annual average wind speed (c), and average sunshine hours (d) during the winter half-year at Lake Daihai from 1960 to 2022.

measured meteorological metrics, surface downward solar radiation and surface downward thermal radiation from the ERA5-Land reanalysis data set also exhibited no significant changes.

3.2. Model Performance

The performance of the FVCOM-CICE model was evaluated using measured hydrometeorological data prior to its application in quantitatively analyzing the drivers of ice-thinning in Lake Daihai.

3.2.1. Lake Ice Simulation

Referring to previous evaluations of the performance of three-dimensional ice models (Oveisy et al., 2012; Wu, Huang, et al., 2023), the measured lake ice thickness at the ice monitoring site was compared with the simulated ice thickness in the grid corresponding to the computational mesh cell where the site is located. Additionally, we calibrated and validated the model using 9 years of measured lake ice thickness to compensate for the scarcity of monitoring points.

Calibration: Measured lake ice thickness data from 1961 to 1986 were used to calibrate the model by iteratively adjusting key parameters to determine the optimum parameter configuration for the model. Ye et al. (2019) have specifically discussed the key parameters (i.e., the ice albedo and vertical Prandtl number) of the FVCOM-CICE model. Based on their study, the ice albedo was dynamically calculated based on the water temperature and ice thickness using the default ice module in the FVCOM-CICE model, but the vertical Prandtl number was determined by model calibration. The vertical Prandtl number was calibrated to 2, which is within the range of 1–10 reported by Ye et al. (2019). Except these two parameters, the other parameters were set to their default values in the FVCOM-CICE model (Chen et al., 2012; Fujisaki-Manome et al., 2020). Using this parameter

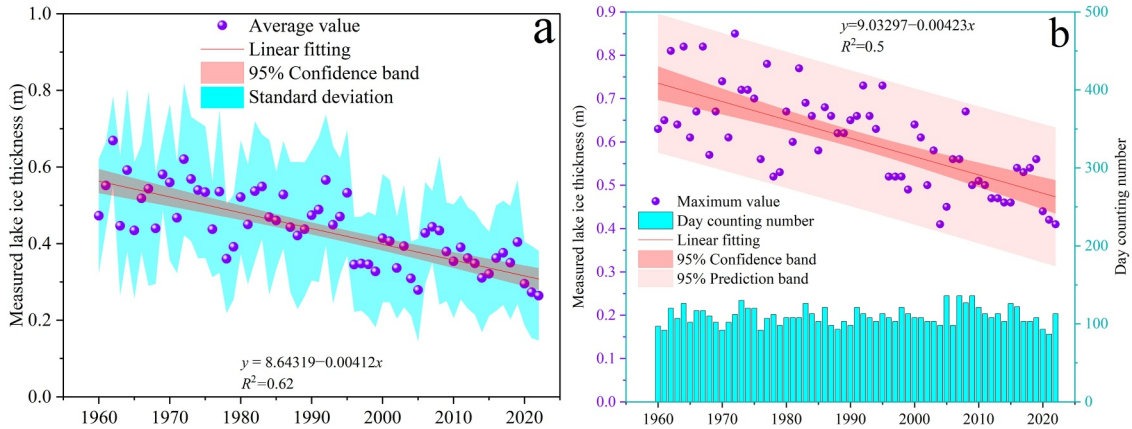

Figure 7. Variations in the measured lake ice thickness in Lake Daihai in the winter half-year from 1960 to 2022: average, standard deviation and fitting curve with confidence band (a); maximum, day counting number corresponding to the annual maximum ice thickness, and fitting curve with the confidence band and prediction band (b).

configuration, the model achieved average values of the performance metrics during the calibration period of $R = 0.95$, BIAS = 2.1 cm, and MBD = 4.5% (Figures 8a and 8b).

Validation: The performance of the calibrated model was evaluated using independent ice thickness measurements from 1991, 1996, 2001, 2006, 2011, 2016, and 2021. The model reliably reproduced the lake ice phenological cycles in years unaffected by thermal effluent discharge pollution, including 1991 (Figure 8c), 1996 (Figure 8d), 2001 (Figure 8e), and 2021 (Figure 8i). The validation results showed favorable performance metrics

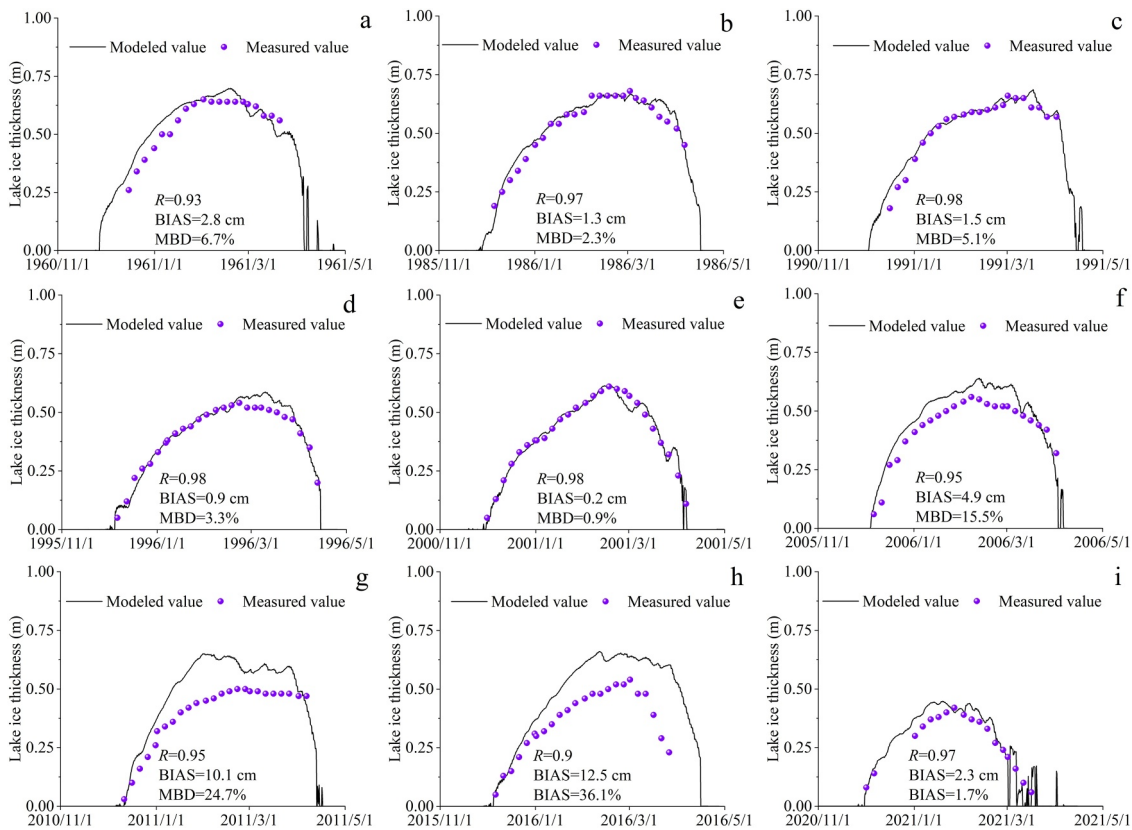

Figure 8. Comparisons between modeled and measured time series of lake ice thickness for Lake Daihai (1961 (a), 1986 (b), 1991 (c), 1996 (d), 2001 (e), 2006 (f), 2011 (g), 2016 (h), and 2021 (i)).

(BIAS = 1.1 cm; MBD = 2%), outperforming existing three-dimensional numerical models applied to simulate lake ice dynamics (BIAS = 8.2 cm, Wu, Huang, et al., 2023; MBD = 21.2%, Oveisy et al., 2012).

The ice dynamics from the Sentinel-2 satellite images and the ice thickness and flow speed simulated by the FVCOM-CICE model are shown in Figure 9. The satellite imagery and model results show good agreement and indicated that Lake Daihai was completely frozen during three months (December, January, and February) in the winter half-year of 2020–2021, while the ice freezing and melting processes occurred primarily in late autumn (November) and early spring (March). Although no satellite images record the ice freezing process in 2020–2021, both the satellite images and the model revealed that westerly winds drove the downwind drift of the lake ice during the ice melting process and subsequent accumulation in the southeastern lake area. This process led to an earlier onset of the ice-free period in upwind lake areas and delayed ice break-up in downwind regions. These spatial patterns align well with the established understanding of lake ice behavior (Wu, Huang, et al., 2023).

However, the model exhibited a systematic overestimation of the lake ice thickness in 2006 (Figure 8f), 2011 (Figure 8g), and 2016 (Figure 8h). This discrepancy stems from the thermal effluent from the Daihai power plant discharging into the lake since 2005 (Chun et al., 2020; Figure 10). The thermal effluent discharge increased the lake water temperature, suppressed ice formation, and accelerated ice melt, causing the escalating model errors observed in 2006, 2011, and 2016. A comparative analysis of the simulated versus measured values of ice thickness reveals that thermal effluent discharge induced decreases in ice thickness of 10.2% (2006), 21.3% (2011), and 23.8% (2016). The reduction in ice thickness in 2006 was only half that in 2011 or 2016 because the Daihai Power Plant was in its trial operation phase in 2005, when the thermal effluent discharge was relatively low.

3.2.2. Water Temperature Simulation

Daily water temperatures measured from May 1996 and 2001 were utilized to validate the model. The results demonstrated that the model successfully simulated the warming processes of surface water temperature (Figure 11). However, the measured water temperature exhibited significantly greater fluctuations in amplitude than the model outputs. This discrepancy likely originates from the vertical resolution of the model and wind wave-induced mixing processes.

Control experiments revealed the formation of a strong inverse water temperature profile (IWTP) during the freeze-over period (Figure 12), characterized by an increase in water temperature from the freezing point at the surface to approximately 4°C near the lakebed. This IWTP increased the vertical stability of the water column and facilitated the development and maintenance of the ice cover throughout the winter. As the air temperature increased in spring, the IWTP gradually weakened, leading to lake water overturn by increasing vertical mixing, followed by the rapid warming of surface lake water. These patterns are consistent with observations in other shallow ice-covered lakes (Bouffard et al., 2019; Huang et al., 2021; Kirillin et al., 2021; Lazhu et al., 2021). However, snowfall—primarily occurring in February and March—slowed the rise in water temperature and delayed the lake water overturn in Lake Daihai. In addition, the simulated water temperature in the near-bed warmer layer ranged from 2.7 to 3.4°C in January 2021, which aligns closely with the contemporaneous in situ measurement of 1–3°C reported by Wu, Liu, et al. (2023) for Lake Daihai. Salinity is the main factor that maintains the low water temperature beneath the ice cover.

3.3. Results of the Model Experiments

3.3.1. Relative Importance of the Influencing Factors

Modeled ice metrics from salinity experiments significantly decreased from 1961 to 2021 ($p < 0.01$; Table 2), except for the increase of the ice-on date. Similarly, the maximum ice thickness from the control experiments and the average ice thickness and duration from the air temperature experiments also decreased significantly ($p < 0.05$; Table 2). No significant changes were observed in the remaining ice metrics from the other model experiments listed in Table 2.

The correlation analysis revealed that the modeled ice thickness was significantly negatively correlated with the average water depth ($r = -0.93$; $p < 0.01$), water salinity ($r = -0.99$; $p < 0.01$), and air temperature ($r = -0.86$; $p < 0.01$). In contrast, no significant correlation was detected with the lake area or wind speed (Figure 13). Additionally, the ice-on date was positively correlated with both the average water depth ($r = 0.97$; $p < 0.01$) and

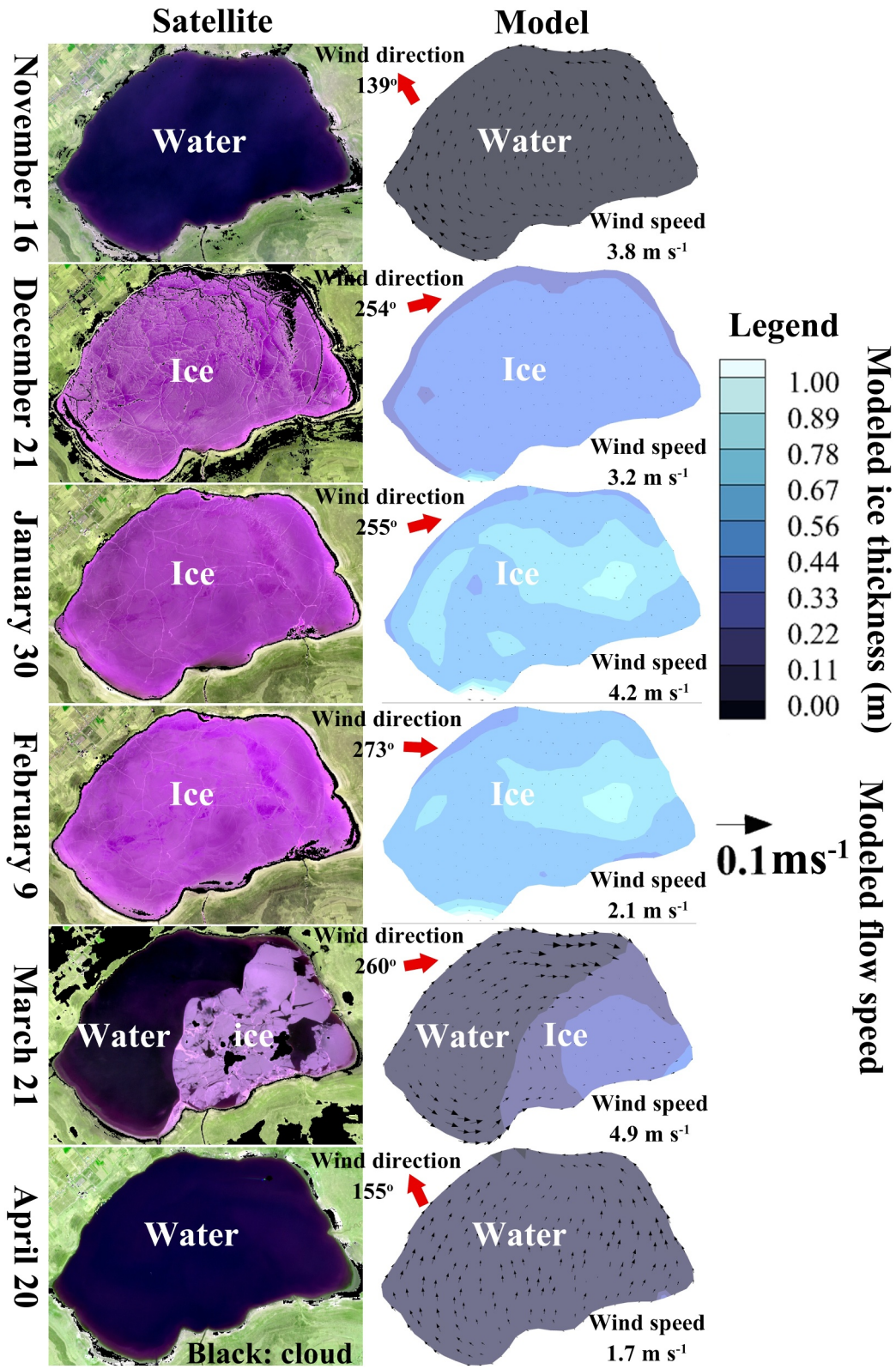

Figure 9. Freezing/melting processes of Lake Daihai in the winter half-year of 2020–2021. Left column: Sentinel-2 satellite images with false color composite bands 2-4-8. Right column: model simulations with the legend showing the color shading depicting the ice thickness.

10.1029/2024WR038954

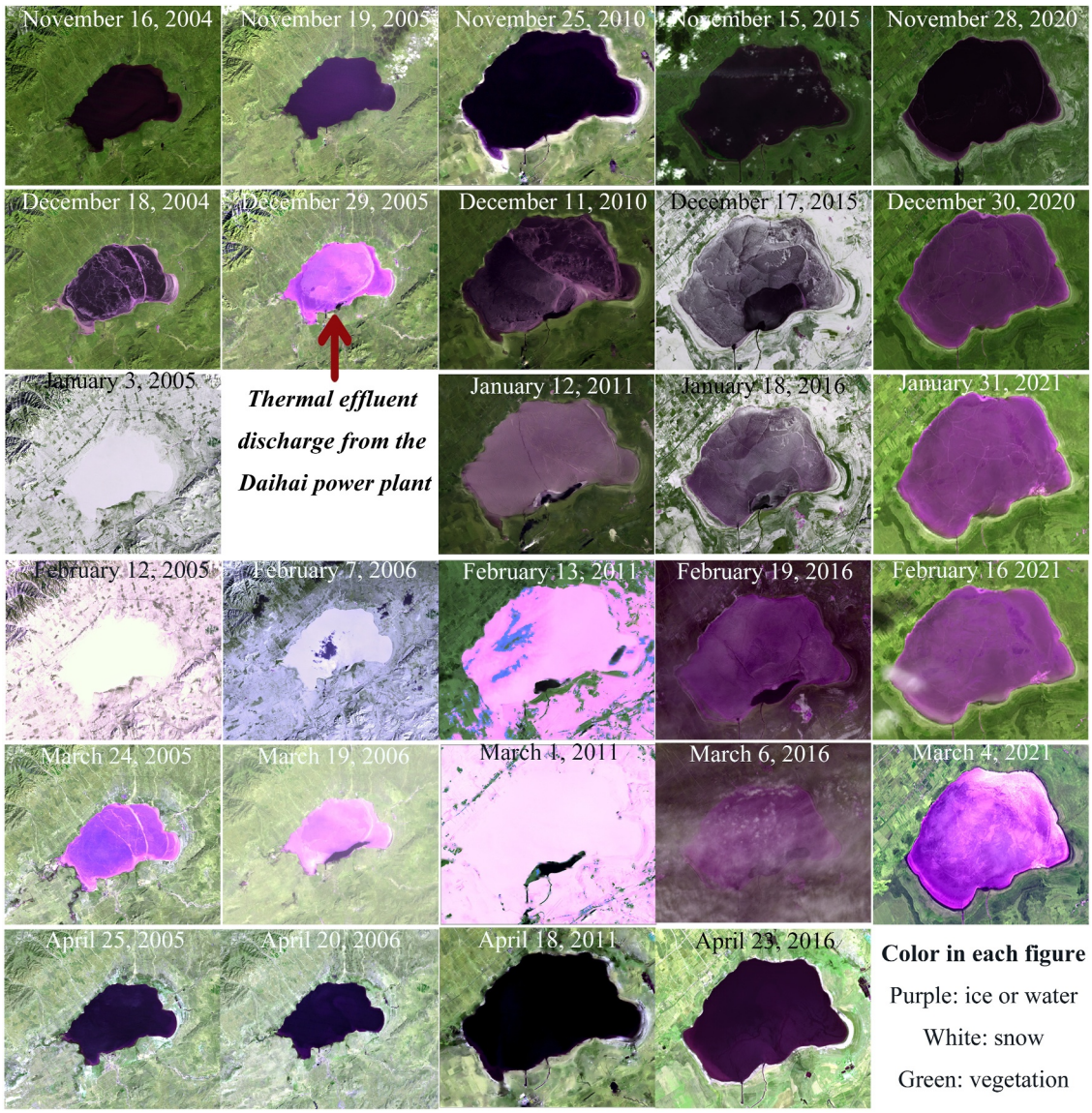

Figure 10. Lake ice cycles of Lake Daihai (2004–2021) derived from TM/ETM + images showing the influences of thermal effluent discharge from the Daihai Power Plant on lake ice dynamics (2005–2019).

salinity ($r = 0.98$; $p < 0.01$), whereas the ice-off date was negatively correlated with these factors ($r = -0.97$ and $r = -0.96$, respectively; $p < 0.01$ for both). These results suggest that ice-thinning was attributed mainly to salinization, atmospheric warming, and lake shrinkage characterized by a decrease in the average water depth. Furthermore, decreasing wind speeds had no significant influence on the ice thickness or phenological metrics, as indicated by the minimal changes in average ice thickness from the wind speed experiments (Figures 13g and 13h).

The measured values of salinity, air temperature, and average ice thickness in 1961 and 2021 closely matched those estimated by the regression equations shown in Figures 6a and 6b and 7a. Therefore, the modeled average ice thickness for these two years was compared to quantify the rates of the contributions of the average water depth, salinity, and air temperature to the ice thinning observed from 1961 to 2021. Control experiments indicated a 42.8% decrease in annual total ice thickness (i.e., average ice thickness × ice duration) over this period. The attribution analysis revealed that air temperature accounted for 36.1% of this decrease, salinity accounted for 18.9%, wind speed accounted for 3.5%, and average water depth accounted for −15.2% (Figure 14a), with the remaining −0.5% attributed to other factors. Additionally, compared with the control–1961 experiments, the

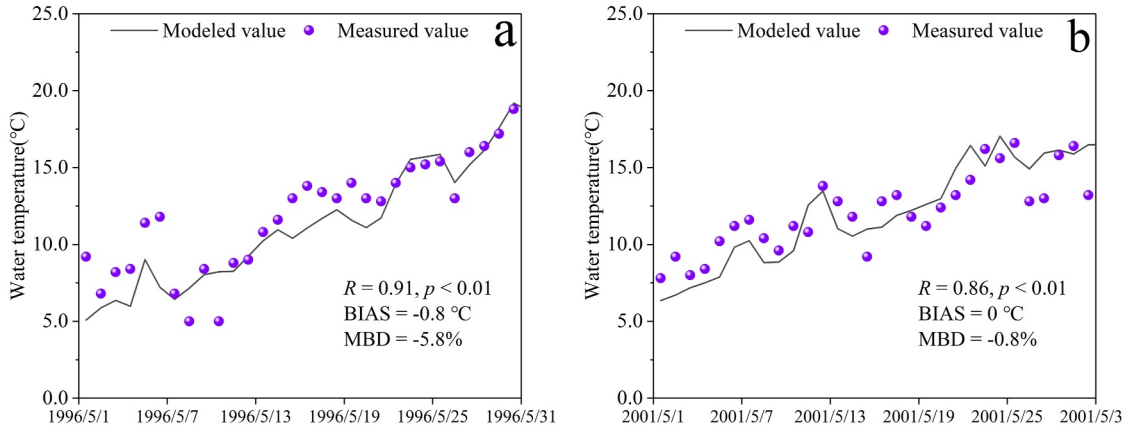

Figure 11. Temporal changes in water temperature measured at a water depth of 20 cm below the lake surface compared with the modeled water temperature of the surface water layer during (a) May 1996 and (b) May 2001.

morphology–2021 experiments revealed earlier ice-on dates and later ice-off dates (Figure 14b), whereas the salinity–2021 and air temperature–2021 experiments produced opposite trends. These results suggest that while atmospheric warming was the dominant driver of ice thinning in Lake Daihai, lake shrinkage (i.e., a reduction in average water depth) slowed this process.

3.3.2. Forecast Experiments

Without effective intervention, Lake Daihai is projected to undergo substantial changes by 2031: the lake area is expected to decrease to 30.8 km^2, with an average water depth of 1.57 m; the salinity is predicted to increase to 18.19‰, corresponding to a salinization rate of 0.51‰ yr^{-1} in the third lake shrinking phase; and the average air temperature in the winter half-year is predicted to increase by 2.8°C. Based on these projections, forecasted all–2031 indicated that the average ice thickness would decrease to 13.9 cm, the ice-on date would be delayed to mid-December, and the ice-off date would advance to late February (Figure 15). Compared with the 1961 baseline, the projected changes in air temperature, salinity, and average water depth account for 35.7%, 67.3%, and −25.6%, respectively, of the reduction in average ice thickness. These results underscore that salinization will become the dominant driver of ice evolution in the near future.

4. Discussion

Lake Daihai was selected as a prototype system to investigate the response of lake ice to global warming in endorheic basins, with a particular emphasis on the effects of lake shrinkage. This lake underwent accelerated shrinkage from 1960 to 2022 accompanied by progressive salinization. Concurrently, the annual average ice thickness also exhibited a pronounced decreasing trend. This ice-thinning trend was attributed to the processes of atmospheric warming (air temperature rise: 2.5°C), salinization (salinity rise: 451.3%), and morphological changes associated with lake shrinkage (water level decrease: 12 m; surface area reduction: 72.9%). Model experiments confirmed significant correlations between the ice thickness and phenological metrics with the air temperature, salinity, and average water depth. Future projections suggest that ice thinning will intensify by 2031 because of the combined impacts of atmospheric warming, salinization, and lake shrinkage.

4.1. Lake Shrinkage

As a closed lake, the water balance of Lake Daihai is governed by direct precipitation and allogenic inflows, while water loss occurs solely through surface evaporation (Wang et al., 2022). Precipitation–evaporation dynamics are quantitatively reflected by interannual water level fluctuations and areal changes from 1960 to 2022 (Figure 14). A notable example is the short lake recovery phase between 2002 and 2005. This recovery phase followed a period of sustained moisture deficit (1997–2001: precipitation = 335.9 ± 50.3 mm, evaporation = 986.1 ± 22.2 mm) and was followed by a shift to a wetter climatic period (2002–2005: precipitation = 508.5 ± 122.0 mm, peaking at 669.4 mm in 2003; evaporation = 949.7 ± 52.9 mm) during which the water level and lake area increased by 0.74 m and 2.2 km^2, respectively.

10.1029/2024WR038954

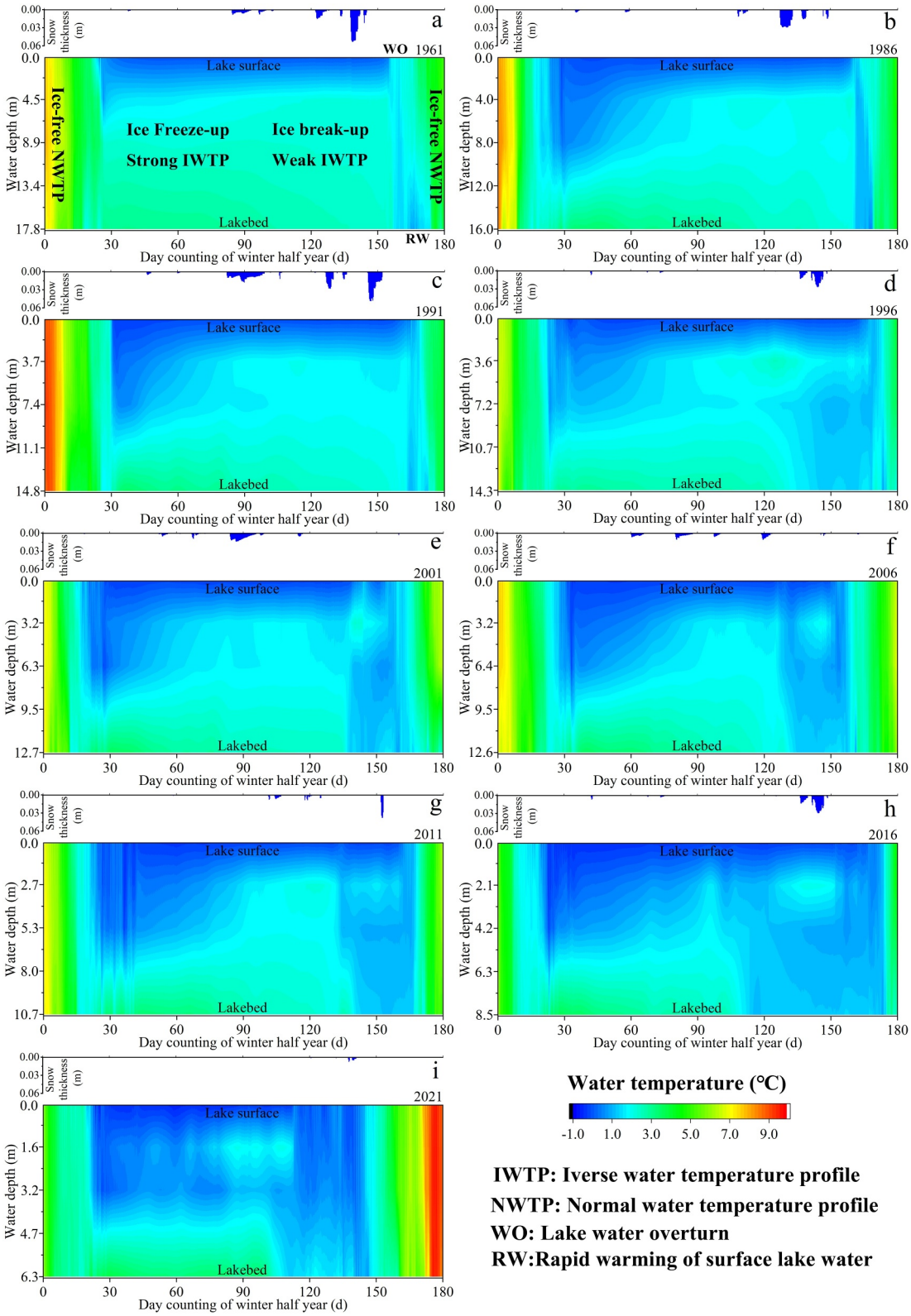

Figure 12. Temporal variations in simulated water temperature profiles at the deepest point and snow thickness in control experiments from 1 day (preceding November 1) to 180 or 181 days (April 30) for 1961 (a), 1986 (b), 1991 (c), 1996 (d), 2001 (e), 2006 (f), 2011 (g), 2016 (h), and 2021 (i).

Table 2
Average and Maximum Lake Ice Thicknesses, Ice-On Date, Ice-Off Date, and Ice Duration From Control, Morphology, Salinity, Air Temperature, and Wind Speed Experiments for the Years 1961, 1986, 1991, 1996, 2001, 2006, 2011, 2016, and 2021

	Ice thickness (cm)		Ice phenology		
Experiments	Average	Maximum	Ice-on date	Ice-off date	Ice duration (days)
Control	47.2 ± 5.1	66.6 ± 5.3↓	31.5 ± 4.5	164.1 ± 8.6	132.8 ± 8.0
Morphology	53.9 ± 2.8	75.5 ± 4.0	25.1 ± 0.4↓	164.9 ± 0.9	140 ± 1.3
Salinity	49.3 ± 2.5↓	68.5 ± 3.5↓	26.1 ± 0.5↑	163.2 ± 0.9↓	137.4 ± 1.4↓
Air temperature	46.9 ± 3.9↓	66.7 ± 4.4	30.3 ± 4.1	161.5 ± 7.1	131.4 ± 7.2↓
Wind speed	51.9 ± 1.0	72.5 ± 1.4	25.7 ± 0.2	164.6 ± 0.4	139.1 ± 0.5

Note. Arrows indicate significant trends from 1961 to 2021: ↑indicates an increase and ↓ indicates a decrease.

The hydrometeorological analysis revealed nonstationary precipitation–evaporation dynamics during 1960–2022, characterized by decadal-scale oscillations without statistically significant secular trends (Figure 16). These inherent variability patterns inadequately explain the accelerated lake shrinkage. Although Wang et al. (2022) employed a distributed hydrological model to reconstruct naturalized streamflow, their simulations similarly showed no significant reduction in discharge. Instead, they attributed the shrinkage to the diversion of runoff for regional economic activities (e.g., agricultural irrigation, industrial water consumption, and reservoir storage). Our study further demonstrates that the three phases of water level variation (slow decrease, moderate decrease, and rapid decrease) in Lake Daihai closely align with major socioeconomic policy shifts in China: the initial development (1950–1977), the Reform and Opening-Up era (1978–2004), and the Western Development Strategy (2005–the present). This synchronicity underscores the profound effects of national-scale water resource management strategies on the sustainability of closed lakes.

The role of anthropogenic factors in driving the shrinkage of Lake Daihai has been well documented (Chen et al., 2020; Chun et al., 2020; Feng et al., 1994); however evaporative forcing also constitutes a significant hydrologic stressor. Notably, thermal effluent discharge from the Daihai Power Plant had increase the water temperature across the lake (Chun et al., 2020), thereby increasing the evaporative flux and accelerating lake shrinkage. This effect is quantitatively corroborated by the accelerated salinization after 2005 (salinity rise: 451.3%). Crucially, anthropogenically diverted water is ultimately lost to the atmosphere through evaporation rather than productive reuse, establishing evaporation as a critical amplifier of lake shrinkage.

4.2. Lake Ice Thinning Process

Consistent with the global trend observed in many ice-covered lakes (Huang et al., 2022; Magnuson et al., 2000; Sharma et al., 2019), Lake Daihai experienced an ice-thinning process along with the decline of water level. The average decreasing rate of −0.39 cm yr^{-1} exceeds the decreasing rates of other lakes which ranged from −0.9 cm $decade^{-1}$ to 2.8 cm $decade^{-1}$ (Choiński et al., 2013; Korhonen, 2006; Magee et al., 2016). Lake ice dynamics depends on meteorological metrics, water salinity, water temperature, and lake morphologic metrics (Korhonen, 2006; Leppäranta, 2023). The regression analysis revealed that solar radiation did not change during the 63-year observation period, whereas the results of the wind speed experiments confirmed that the changes in the wind speed minimally affected the ice thickness and phenological metrics. Thus, Thus, the accelerated ice-thinning in Lake Daihai is primarily attributable to long-term changes in air temperature, salinity, and lake morphometry.

Global declines in lake ice cover have been conclusively attributed to anthropogenic climate change through shifts in thermal–atmospheric regimes (Grant et al., 2021; Huang et al., 2022; Lehnherr et al., 2018; Sharma et al., 2019; Woolway et al., 2020). A key characteristic of these changes is atmospheric warming, as manifested by rising air temperatures. Our analysis revealed a negative correlation between the lake ice thickness and air temperature. Model experiments further confirmed these thermal–atmospheric linkages, indicating that atmospheric warming contributed to a 36.1% reduction in lake ice thickness in 2021. These findings align with the well-established scientific understanding that the thermodynamic influence of air temperature on lake ice via

10.1029/2024WR038954

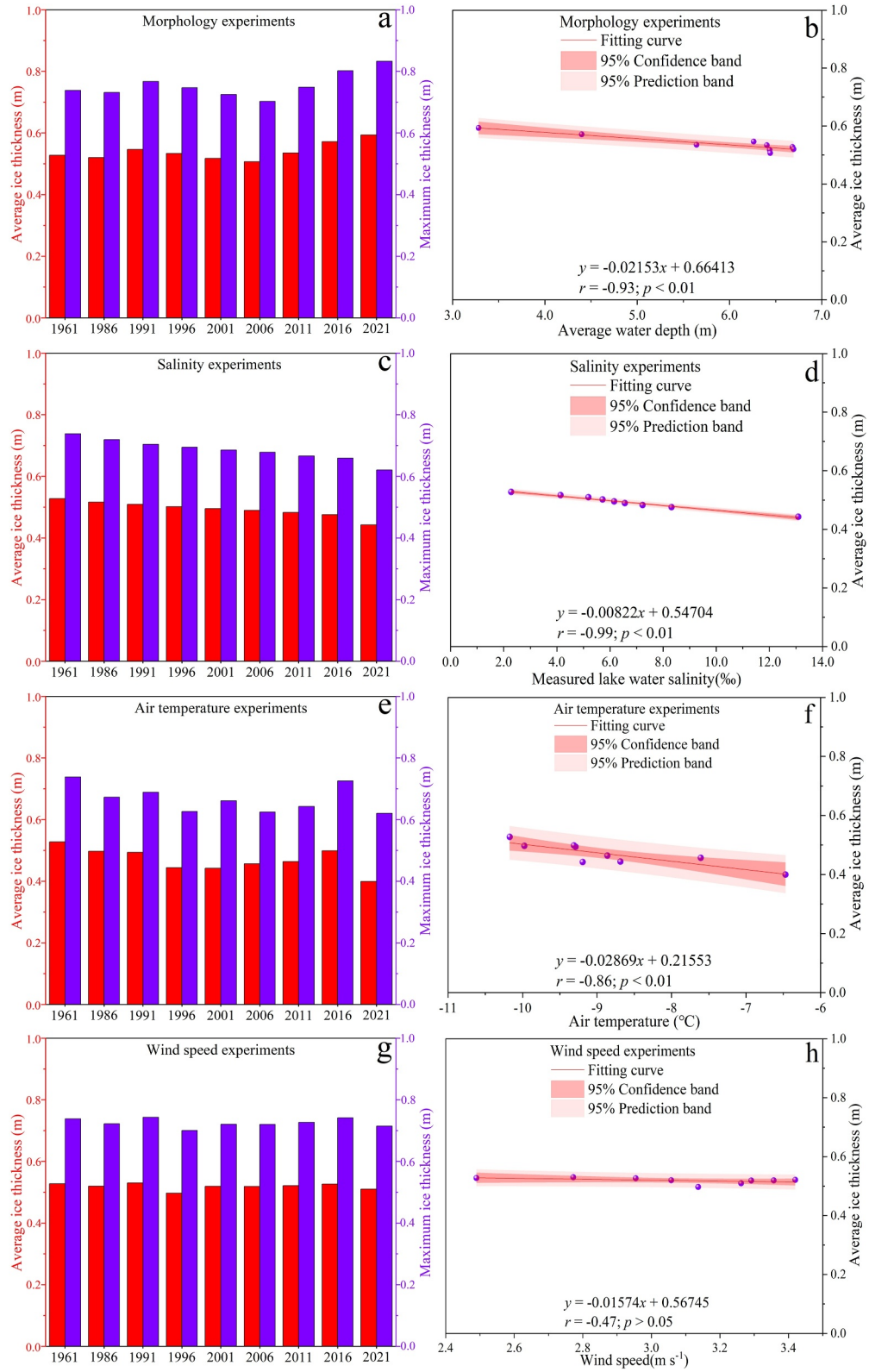

Figure 13. Modeled average and maximum ice thicknesses from (a) morphology, (c) salinity, (e) air temperature, and (g) wind speed experiments.; Correlations between the average ice thickness and (b) average water depth, (d) salinity, (f) air temperature, and (h) wind speed.

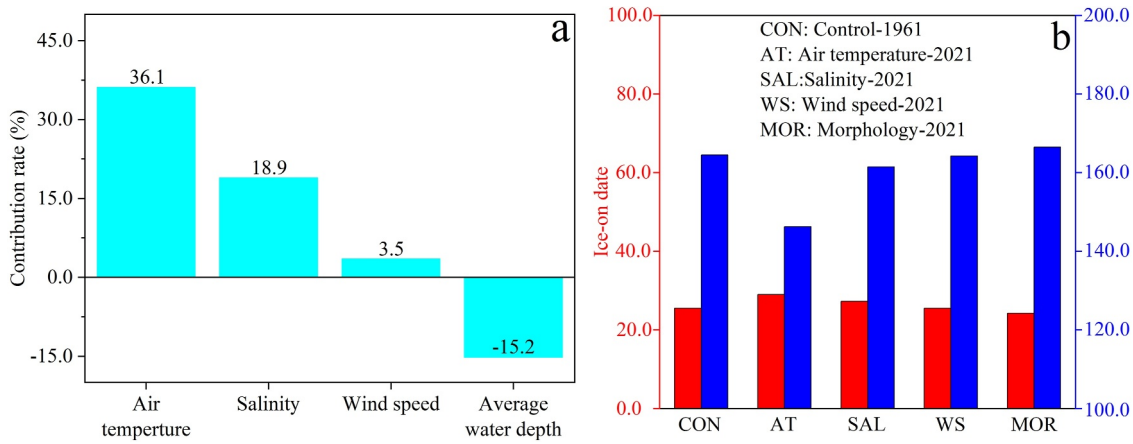

Figure 14. Contributions of changes in air temperature, salinity, wind speed, and morphology (average water depth) to (a) decreases in ice thickness and (b) variations in ice phenological metrics between the control–1961 experiment and model experiments for 2021.

sensible heat flux modulation (Gebre et al., 2014; Leppäranta, 2023; Sharma et al., 2019; Xu et al., 2024). Although solar radiation and wind speed are theoretically capable of influencing ice thermal dynamics, our study revealed no evidence that these factors contributed significantly to ice-thinning in Lake Daihai.

Salinity (S) plays a critical role in lake ice dynamics by regulating the ice freezing point temperature ($T_f = -0.054S$). A higher salinity lowers the freezing point, making saline water more resistant to ice formation than freshwater (Leppäranta, 2023; Pieters & Lawrence, 2009). This mechanism explains why Chaka Salt Lake (salinity: ~330‰) remains ice-free throughout the year, while its neighboring Qinghai Lake (salinity: 14.1‰) freezes annually in winter (Shi et al., 2024). Our salinity experiments further support this conclusion, showing that compared with the conditions in 1961, the salinity level in 2021 contributed to an 18.9% reduction in lake ice thickness. The contribution of salinity to the decrease in ice thickness is projected to increase markedly, reaching 60% by 2031, indicating a nonlinear intensification of the effects of salinization on ice thinning. Salinization increases the energy loss threshold required for lake freezing in winter and reduces the energy absorption threshold needed for spring melting, whereas atmospheric warming suppresses the upward heat flux and increases the downward heat flux at the air–ice or air–water interface. Through persistent atmospheric warming, the nonlinear intensification of salinization is projected to further accelerate the decline in the annual lake ice cycle in Lake Daihai in the near future.

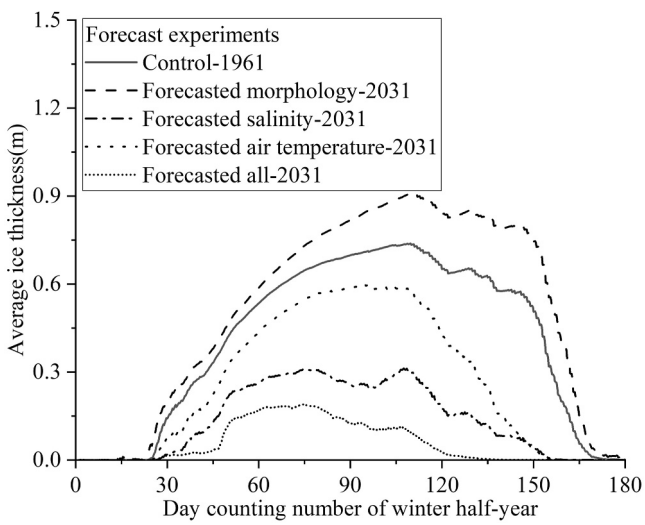

Figure 15. Temporal variations in the simulated average ice thickness from forecast experiments during the winter half-year quantified using the number of days (starting from November 1).

Conversely, lake shrinkage slowed ice thinning in Lake Daihai. Morphological experiments indicated that decreases in lake morphological metrics (e.g., average water depth) contributed to increases in the ice thickness and duration, with a contribution rate of −15.2%. However, a reduction in the lake area does not necessarily lead to thicker lake ice, as the two variables exhibit no significant relationship. The lake area even shows a significant positive correlation with the measured annual average ice thickness. These findings help explain why some studies (Smits et al., 2021; Williams & Stefan, 2006) have reported minimal impacts of lake morphology on ice phenological patterns. A decrease in the water level reasonably results in a decrease in the lake area, but it also possibly leads to an increase in the average water depth by decreasing the proportion of shallow-water areas (Figures 3 and 5). For instance, Lake Daihai had a larger surface area in 1991 (112.3 km^2) than in 2006 (80.8 km^2), yet its average water depth was shallower in the earlier year (6.26 vs. 6.44 m in 2006). This discrepancy can be attributed to the greater proportion of shallow-water areas in 1991 than in 2006.

The proportion of shallow-water areas is a key variable influencing lake ice phenology. For instance, Lake Huron has the earliest median first-ice date and the latest last-ice date among the Great Lakes, resulting in the longest typical

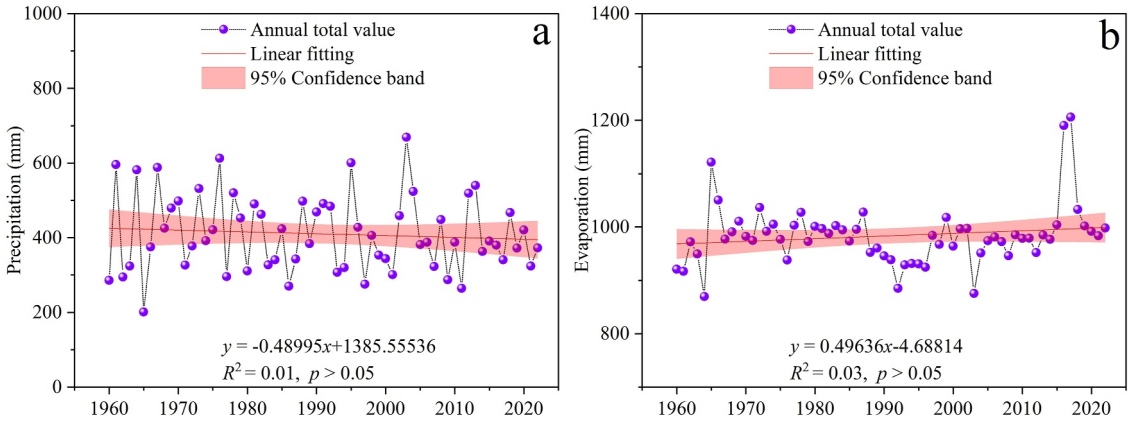

Figure 16. Interannual variations in panel (a) total precipitation and (b) evaporation at Lake Daihai from 1960 to 2022.

ice cycle duration, which can be attributed to its extensive shallow areas (Assel, 2005). This process occurs because the heat storage capacity is significantly lower in shallow regions than in deeper areas. Morphology experiments indicated that the unit area heat content of Lake Daihai in 1991 (3.88×10^{16} J km^{-1}) was lower than that in 2006 (4.09×10^{16} J km^{-1}), corresponding to greater ice thickness and a longer duration in the earlier year. Sharma et al. (2019) also observed that deep large lakes are more likely to lose ice cover than shallow small lakes Compared with water columns with higher heat contents, water columns with lower heat contents are more prone to freezing and are more difficult to melt (Williams et al., 2004). A greater amount of heat stored beneath the convective mixing layer can more effectively suppress ice growth and accelerate ice breakup through upward thermal diffusion (Aslamov et al., 2014; Ellis et al., 1991; Huang et al., 2019). This finding explains why the ice phenological metrics are significantly correlated with the average water depth rather than with the lake surface area. Similarly, Sharma et al. (2019) further highlighted that the mean depth plays a critical role in determining the probability of ice decline among lakes at comparable latitudes.

4.3. Potential Future Changes

If no countermeasures are implemented to mitigate water loss, Lake Daihai is projected to desiccate by approximately 2055 using the regression equation of the lake area presented in Figure 4b. Global warming is expected to further accelerate this process by increasing evaporation and reducing lake ice (Wang, Lee, et al., 2018; Woolway et al., 2020). Forecast experiments suggest that the average ice thickness in 2031 will decrease to 38.8% of that in 2021 and that the ice duration will shorten to 68.3 days under the combined effects of atmospheric warming, salinization, and lake shrinkage. The ice-thinning rate between 2021 and 2031 is projected to be dramatically greater than that observed between 1961 and 2021. Furthermore, shorter ice durations enhance lake evaporation, which subsequently accelerates lake shrinkage and salinization (Leppäranta, 2023; Woolway & Merchant, 2019). This process creates a self-perpetuating feedback cycle that will likely cause Lake Daihai to become ice-free earlier than anticipated and eventually lead to its complete drying before 2055.

In addition, given the rapid decrease in water storage in lakes on the Mongolian Plateau where Lake Daihai is located (Tao et al., 2015), projections of lake ice changes in this semiarid region must rigorously account for the influences of lake shrinkage and salinization on ice dynamics. Salinity and morphology experiments revealed that the lake ice thickness was underestimated when salinization was overlooked, whereas it was overestimated when the decrease in the average water depth in Lake Daihai was ignored. This conclusion is also relevant for lakes undergoing rapid water storage changes globally (Wang, Song, et al., 2018).

5. Conclusions

Lake Daihai underwent intensive shrinkage, with an areal recession rate of −2.18 km^2 yr^{-1} from 1960 to 2022, which was driven by increasing anthropogenic activities and increased evaporation. Concurrently, the measured lake ice thickness in the winter half-year decreased rapidly from 0.47 ± 0.15 m in 1960 to 0.26 ± 0.12 m in 2022, which is equivalent to an average decreasing rate of −0.39 cm yr^{-1}. This ice-thinning trend was the result of the

combined effects of atmospheric warming, salinization, and morphological changes (i.e., a decrease in the average water depth). Model experiments revealed that ice phenological metrics were significantly correlated with these drivers. Atmospheric warming and salinization contributed positively to ice thinning, accounting for 36.1% and 18.9%, respectively, of the observed ice thinning, while the decrease in the average water depth partially mitigated ice thinning by reducing the heat content capacity of the lake (−15.2% of ice-thinning). Forecast experiments indicate that the ice thickness and duration in 2031 are projected to decrease rapidly to 61.3% and 60.4% of those in 2021, respectively. Concurrently, lake ice-thinning further reduced the ecosystem services provided by Lake Daihai.

This study has several limitations. First, water temperature and heat content during ice-free periods were not considered, and simulations for 2006, 2011, and 2016 lack adequate validation because of the unavailability of data pertaining to the Daihai Power Plant. Second, reconstructing lake ice dynamics annually from 1960 to 2022 allows for a more thorough analysis of the drivers of ice thinning than reconstructing it for the nine discrete years examined in this study. Third, as in-depth understanding of lake ice dynamics improves, lake ice numerical models will be further developed to help us quantify the contributions of various driving factors to lake ice more accurately. Therefore, further research is needed to address these gaps.

Conflict of Interest

The authors declare no conflicts of interest relevant to this study.

Data Availability Statement

The FVCOM-CICE model (FVCOM 5.0.1) is available in the website of https://github.com/FVCOM-GitHub/FVCOM. Field data, model, and model results are available at website of https://data.mendeley.com/drafts/j796j4ykfz.

Acknowledgments
This study was supported by the National Natural Science Foundation of China (Nos. 52525902, 52121006, 52279018, 41971047), Fundamental Research Funds for the Central Universities (B250201135, B240201015-2013) and the authors thank Prof. James C. McWilliams from UCLA and Prof. Wenfeng Huang from Chang'an University for scientific suggestions, Prof. Yu Liu from Inner Mongolia Agricultural University, and Prof. Xi Chun from Inner Mongolia University for data collection.

References

Anderson, E. J., Fujisaki-Manome, A., Kessler, J., Lang, G. A., Chu, P. Y., Kelley, J. G. W., et al. (2018). Ice forecasting in the next-generation great lakes operational forecast system (GLOFS). *Journal of Marine Science and Engineering*, *6*(4), 123. https://doi.org/10.3390/jmse6040123

Anderson, E. J., Schwab, D. J., & Lang, G. A. (2010). Real-time hydraulic and hydrodynamic model of the St. Clair River, Lake St. Clair, Detroit River System. *Journal of Hydraulic Engineering*, *136*(8), 507–518. https://doi.org/10.1061/(asce)hy.1943-7900.0000203

Arp, C. D., Whitman, M. S., Jones, B. M., Nigro, D. A., Alexeev, V. A., Gädeke, A., et al. (2019). Ice roads through lake-rich Arctic watersheds: Integrating climate uncertainty and freshwater habitat responses into adaptive management. *Arctic Antarctic and Alpine Research*, *51*(1), 9–23. https://doi.org/10.1080/15230430.2018.1560839

Aslamov, I. A., Kozlov, V. V., Kirillin, G. B., Mizandrontsev, I. B., Kucher, K. M., Makarov, M. M., et al. (2014). Ice–water heat exchange during ice growth in Lake Baikal. *Journal of Great Lakes Research*, *40*(3), 599–607. https://doi.org/10.1016/j.jglr.2014.06.004

Assel, R. (2005). Classification of annual Great Lakes ice cycles: Winters of 1973-2002. *Journal of Climate*, *18*(22), 4895–4905. https://doi.org/10.1175/jcli3571.1

Bai, P., Wang, J., Chu, P., Hawley, N., Fujisaki-Manome, A., Kessler, J., et al. (2020). Modeling the ice-attenuated waves in the Great Lakes. *Ocean Dynamics*, *70*(7), 991–1003. https://doi.org/10.1007/s10236-020-01379-z

Bernhardt, J., Engelhardt, C., Kirillin, G., & Matschullat, J. (2012). Lake ice phenology in Berlin-Brandenburg from 1947–2007: Observations and model hindcasts. *Climatic Change*, *112*(3–4), 791–817. https://doi.org/10.1007/s10584-011-0248-9

Blagrave, K., & Sharma, S. (2023). Projecting climate change impacts on ice phenology across midwestern and Northeastern United States lakes. *Climatic Change*, *176*(9), 119. https://doi.org/10.1007/s10584-023-03596-z

Bouffard, D., Zdorovennova, G., Bogdanov, S., Efremova, T., Lavanchy, S., Palshin, N., et al. (2019). Under-ice convection dynamics in a boreal lake. *Inland Waters*, *9*(2), 142–161. https://doi.org/10.1080/20442041.2018.1533356

Briegleb, B., Bitz, C., Hunke, E., Lipscomb, W., & Schramm, J. (2002). *Description of the community climate System model version 2: Sea ice model*. UCAR.

Brown, L. C., & Duguay, C. R. (2010). The response and role of ice cover in lake-climate interactions. *Progress in Physical Geography*, *34*(5), 671–704. https://doi.org/10.1177/0309133310375653

Brown, L. C., & Duguay, C. R. (2011). The fate of lake ice in the North American Arctic. *The Cryosphere*, *5*(4), 869–892. https://doi.org/10.5194/tc-5-869-2011

Chen, C., Beardsley, R. C., & Cowles, G. (2012). *An unstructured-grid, finite-volume community ocean model: FVCOM user manual. Cambridge, MA, USA: Sea Grant College Program*. Massachusetts Institute of Technology.

Chen, J., Lv, J., Li, N., Wang, Q., & Wang, J. (2020). External groundwater alleviates the degradation of closed lakes in semi-arid regions of China. *Remote Sensing*, *12*(1), 45. https://doi.org/10.3390/rs12010045

Choiński, A., Ptak, M., & Strzelczak, A. (2013). Areal variation in ice cover thickness on Lake Morskie Oko (Tatra Mountains). *Carpathian Journal of Earth and Environmental Sciences*, *8*(3), 97–102.

Chun, X., Qin, F., Zhou, H., Dan, D., Xia, Y., & Ulambadrakh, K. (2020). Effects of climate variability and land use/land cover change on the Daihai wetland of central Inner Mongolia over the past decades. *Journal of Mountain Science*, *17*(12), 3070–3084. https://doi.org/10.1007/s11629-020-6108-1

Dibike, Y., Prowse, T., Saloranta, T., & Ahmed, R. (2011). Response of Northern Hemisphere lake-ice cover and lake-water thermal structure patterns to a changing climate. *Hydrological Processes*, *25*(19), 2942–2953. https://doi.org/10.1002/hyp.8068

Ellis, C. R., Stefan, H. G., & Gu, R. (1991). Water temperature dynamics and heat transfer beneath the ice cover of a lake. *Limnology & Oceanography*, *36*(2), 324–334. https://doi.org/10.4319/lo.1991.36.2.0324
Fairall, C. W., Bradley, E. F., Hare, J. E., Grachev, A. A., & Edson, J. B. (2003). Bulk parameterization of air-sea fluxes: Updates and verification for the COARE algorithm. *Journal of Climate*, *16*(4), 571–591. https://doi.org/10.1175/1520-0442(2003)016<0571:bpoasf>2.0.co;2
Farmer, T. M., Marschall, E. A., Dabrowski, K., & Ludsin, S. A. (2015). Short winters threaten temperate fish populations. *Nature Communications*, *6*, 7724. https://doi.org/10.1038/ncomms8724
Feng, X., Wang, Y., Wang, Z., & Li, N. (1994). Analysis and discussion on the changes of Lake Daihai. *Inner Mongolia Water Resources*, 55–56.
Fujisaki-Manome, A., Anderson, E. J., Kessler, J. A., Chu, P. Y., Wang, J., & Gronewold, A. D. (2020). Simulating impacts of precipitation on ice cover and surface water temperature across large lakes. *Journal of Geophysical Research: Oceans*, *125*(5), e2019JC015950. https://doi.org/10.1029/2019JC015950
Gao, G., Chen, C., Qi, J., & Beardsley, R. C. (2011). An unstructured-grid, finite-volume sea ice model: Development, validation, and application. *Journal of Geophysical Research*, *116*, 1–15. https://doi.org/10.1029/2010jc006688
Gebre, S., Boissy, T., & Alfredsen, K. (2014). Sensitivity of lake ice regimes to climate change in the Nordic region. *The Cryosphere*, *8*(4), 1589–1605. https://doi.org/10.5194/tc-8-1589-2014
Grant, L., Vanderkelen, I., Gudmundsson, L., Tan, Z., Perroud, M., Stepanenko, V. M., et al. (2021). Attribution of global lake systems change to anthropogenic forcing. *Nature Geoscience*, *14*(11), 849–854. https://doi.org/10.1038/s41561-021-00833-x
Hampton, S. E., Galloway, A. W. E., Powers, S. M., Ozersky, T., Woo, K. H., Batt, R. D., et al. (2017). Ecology under lake ice. *Ecology Letters*, *20*(1), 98–111. https://doi.org/10.1111/ele.12699
Hocke, K., & Kämpfer, N. (2011). Hovmöller diagrams of climate anomalies in NCEP/NCAR reanalysis from 1948 to 2009. *Climate Dynamics*, *36*, 355–364.
Hodgkins, G. A., James II, I. C., & Huntington, T. G. (2002). Historical changes in lake ice-out dates as indicators of climate change in New England, 1850–2000. *International Journal of Climatology*, *22*(15), 1819–1827. https://doi.org/10.1002/joc.857
Hou, C., Li, Y., Li, W., Yu, S., Yin, Z., Guo, Y., & Fan, C. (2024). Spatial and temporal distribution characteristics of nitrogen and phosphorus and analysis of differences with environmental impact factors in Lake Daihai frozen period and no-frozen period. *Journal of Agro-Environment Science*, *43*(7), 1590–1598.
Huang, L., Timmermann, A., Lee, S. S., Rodgers, K. B., Yamaguchi, R., & Chung, E. S. (2022). Emerging unprecedented lake ice loss in climate change projections. *Nature Communications*, *13*(1), 5798. https://doi.org/10.1038/s41467-022-33495-3
Huang, W., Jiang, J., & Wang, R. (1997). Water salinization and countermeasures in Daihai Lake. *Pollution Control Technology*, *10*(3), 127–130.
Huang, W., Zhang, J., Leppäranta, M., Li, Z., Cheng, B., & Lin, Z. (2019). Thermal structure and water-ice heat transfer in a shallow ice-covered thermokarst lake in central Qinghai-Tibet Plateau. *Journal of Hydrology*, *578*, 124122. https://doi.org/10.1016/j.jhydrol.2019.124122
Huang, W., Zhang, Z., Li, Z., Leppäranta, M., Arvola, L., Song, S., et al. (2021). Under-ice dissolved oxygen and metabolism dynamics in a shallow lake: The critical role of ice and snow. *Water Resources Research*, *57*(5), e2020WR027990. https://doi.org/10.1029/2020WR027990
Hunke, E. C., Lipscomb, W. H., Turner, A. K., Jeffery, N., & Elliott, S. (2015). *CICE: The Los Alamos Sea ice model documentation and software user's manual version 5.1 LA-CC-06-012. T-3 Fluid Dynamics Group* (Vol. 675, p. 15). Los Alamos National Laboratory.
Jeffries, M. O., & Morris, K. (2007). Some aspects of ice phenology on ponds in central Alaska, USA. *Annals of Glaciology*, *46*, 397–403. https://doi.org/10.3189/172756407782871576
Kirillin, G., Leppäranta, M., Terzhevik, A., Granin, N., Bernhardt, J., Engelhardt, C., et al. (2012). Physics of seasonally ice-covered lakes: A review. *Aquatic Sciences*, *74*(4), 659–682. https://doi.org/10.1007/s00027-012-0279-y
Kirillin, G. B., Shatwell, T., & Wen, L. (2021). Ice-covered lakes of Tibetan Plateau as solar heat collectors. *Geophysical Research Letters*, *48*(14), e2021GL093429. https://doi.org/10.1029/2021GL093429
Korhonen, J. (2006). Long-term changes in lake ice cover in Finland. *Nordic Hydrology*, *37*(4), 347–363. https://doi.org/10.2166/nh.2006.019
Large, W. G., & Pond, S. (1981). Open ocean momentum flux measurements in moderate to strong winds. *Journal of Physical Oceanography*, *11*(3), 324–336. https://doi.org/10.1175/1520-0485(1981)011<0324:oomfmi>2.0.co;2
Lazhu, Yang, K., Hou, J., Wang, J., Lei, Y., Zhu, L., et al. (2021). A new finding on the prevalence of rapid water warming during lake ice melting on the Tibetan Plateau. *Science Bulletin*, *66*(23), 2358–2361. https://doi.org/10.1016/j.scib.2021.07.022
Lehnherr, I., St. Louis, V. L., Sharp, M., Gardner, A. S., Smol, J. P., Schiff, S. L., et al. (2018). The world's largest High Arctic lake responds rapidly to climate warming. *Nature Communications*, *9*(1), 1290. https://doi.org/10.1038/s41467-018-03685-z
Leppäranta, M. (2023). *Freezing of Lakes and the evolution of their ice cover* (2nd ed.). Springer. https://doi.org/10.1007/978-3-031-25605-9
Li, M., Zhang, M., Yao, Z., Wang, L., Feng, D., Li, W., & Yang, W. (2024). The trend of dissolved oxygen change and influencing factors of typical lakes in cold area during ice-covered period. *Journal of Lake Sciences*, *36*(6), 1806–1819. https://doi.org/10.18307/2024.0627
Liston, G. E., & Hall, D. K. (1995). An energy-balance model of lake-ice evolution. *Journal of Glaciology*, *41*(138), 373–382. https://doi.org/10.3189/s0022143000016245
Magee, M. R., & Wu, C. H. (2017). Effects of changing climate on ice cover in three morphometrically different lakes. *Hydrological Processes*, *31*(2), 308–323. https://doi.org/10.1002/hyp.10996
Magee, M. R., Wu, C. H., Robertson, D. M., Lathrop, R. C., & Hamilton, D. P. (2016). Trends and abrupt changes in 104 years of ice cover and water temperature in a dimictic lake in response to air temperature, wind speed, and water clarity drivers. *Hydrology and Earth System Sciences*, *20*(5), 1681–1702. https://doi.org/10.5194/hess-20-1681-2016
Magnuson, J. J., Robertson, D. M., Benson, B. J., Wynne, R. H., Livingstone, D. M., Arai, T., et al. (2000). Historical trends in lake and river ice cover in the Northern Hemisphere. *Science*, *289*(5485), 1743–1746. https://doi.org/10.1126/science.289.5485.1743
Martynov, A., Sushama, L., & Laprise, R. (2010). Simulation of temperate freezing lakes by one-dimensional lake models: Performance assessment for interactive coupling with regional climate models. *Boreal Environment Research*, *15*, 143–164.
Maykut, G. A., & McPhee, M. G. (1995). Solar heating of the Arctic mixed layer. *Journal of Geophysical Research*, *100*(C12), 24691–24703. https://doi.org/10.1029/95jc02554
McFeeters, S. K. (1996). The use of the Normalized Difference Water Index (NDWI) in the delineation of open water features. *International Journal of Remote Sensing*, *17*(7), 1425–1432. https://doi.org/10.1080/01431169608948714
Meng, S., Yao, Y., Hu, B., Chen, Y., Wang, L., & Liu, Y. (2023). Spatial distribution characteristics of chlorophyll-a concentration in summer and its influencing factors in Lake Daihai of Mengxin Plateau. *Journal of Lake Sciences*, *35*(4), 1255–1267. https://doi.org/10.18307/2023.0419
Morales-Marín, L. A., French, J. R., & Burningham, H. (2017). Implementation of a 3D ocean model to understand upland lake wind-driven circulation. *Environmental Fluid Mechanics*, *17*(6), 1255–1278. https://doi.org/10.1007/s10652-017-9548-6
Nakada, S., Haga, H., Iwaki, M., Mabuchi, K., & Takamura, N. (2021). High-resolution flow simulation in Typhoon 21, 2018: Massive loss of submerged Macrophytes in Lake Biwa. *Progress in Earth and Planetary Science*, *8*(1), 46. https://doi.org/10.1186/s40645-021-00440-9

Oveisy, A., Boegman, L., & Imberger, J. (2012). Three-dimensional simulation of lake and ice dynamics during winter. *Limnology & Oceanography*, *57*(1), 43–57. https://doi.org/10.4319/lo.2012.57.1.0043

Patterson, R. T., & Swindles, G. T. (2015). Influence of ocean–atmospheric oscillations on lake ice phenology in eastern North America. *Climate Dynamics*, *45*(9–10), 2293–2308. https://doi.org/10.1007/s00382-014-2415-y

Pekel, J. F., Cottam, A., Gorelick, N., & Belward, A. S. (2016). High-resolution mapping of global surface water and its long-term changes. *Nature*, *540*(7633), 418–422. https://doi.org/10.1038/nature20584

Pieters, R., & Lawrence, G. A. (2009). Effect of salt exclusion from lake ice on seasonal circulation. *Limnology & Oceanography*, *54*(2), 401–412. https://doi.org/10.4319/lo.2009.54.2.0401

Rafat, A., Pour, H. K., Spence, C., Palmer, M. J., & MacLean, A. (2023). An analysis of ice growth and temperature dynamics in two Canadian subarctic lakes. *Cold Regions Science and Technology*, *210*, 103808. https://doi.org/10.1016/j.coldregions.2023.103808

Ren, X., Yu, R., Kang, J., Lü, C., Wang, R., Li, Y., & Zhang, Z. (2022). Water pollution characteristics and influencing factors of closed lake in a semiarid area: A case study of Daihai Lake, China. *Environmental Earth Sciences*, *81*(15), 393. https://doi.org/10.1007/s12665-022-10526-2

Robertson, D. M., Ragotzkie, R. A., & Magnuson, J. J. (1992). Lake ice records used to detect historical and future climatic changes. *Climatic Change*, *21*(4), 407–427. https://doi.org/10.1007/bf00141379

Sharma, S., Blagrave, K., Magnuson, J. J., O'Reilly, C. M., Oliver, S., Batt, R. D., et al. (2019). Widespread loss of lake ice around the Northern Hemisphere in a warming world. *Nature Climate Change*, *9*(3), 227–231. https://doi.org/10.1038/s41558-018-0393-5

Sharma, S., Lopez, L. S., Basu, A., Blagrave, K., Bazely, D., Bove, G., & Stewart, K. (2023). An introduction to the community lake ice collaboration: A long-term lake ice phenology community science project spanning 1000 lakes and over 30 years. *Limnology and Oceanography Bulletin*, *32*(2), 41–87. https://doi.org/10.1002/lob.10560

Sharma, S., Meyer, M. F., Culpepper, J., Yang, X., Hampton, S., Berger, S. A., et al. (2020). Integrating perspectives to understand lake ice dynamics in a changing world. *Journal of Geophysical Research: Biogeosciences*, *125*(8), e2020JG005799. https://doi.org/10.1029/2020JG005799

Shi, F., Li, X., Zhao, S., Ma, Y., Wei, J., Liao, Q., & Chen, D. (2024). Evaporation and sublimation measurement and modeling of an alpine saline lake influenced by freeze–thaw on the Qinghai–Tibet Plateau. *Hydrology and Earth System Sciences*, *28*(1), 163–178. https://doi.org/10.5194/hess-28-163-2024

Smits, A. P., Gomez, N. W., Dozier, J., & Sadro, S. (2021). Winter climate and lake morphology control ice phenology and under-ice temperature and oxygen regimes in mountain lakes. *Journal of Geophysical Research: Biogeosciences*, *126*(8), e2021JG006277. https://doi.org/10.1029/2021JG006277

Su, Y., Ran, Y., Zhang, G., & Li, X. (2023). Remotely sensed lake area changes in permafrost regions of the Arctic and the Tibetan Plateau between 1987 and 2017. *Science of the Total Environment*, *880*, 163355. https://doi.org/10.1016/j.scitotenv.2023.163355

Tang, H., Cao, H., Yuan, S., Xiao, Y., Jiang, C., & Gualtieri, C. (2020). A numerical Study of hydrodynamic processes and flood mitigation in a large river-lake System. *Water Resources Management*, *34*(12), 3739–3760. https://doi.org/10.1007/s11269-020-02628-y

Tao, S., Fang, J., Zhao, X., Zhao, S., Shen, H., Hu, H., et al. (2015). Rapid loss of lakes on the Mongolian Plateau. *Proceedings of the National Academy of Sciences of the United States of America*, *112*(7), 2281–2286. https://doi.org/10.1073/pnas.1411748112

Walsh, S. E., Vavrus, S. J., Foley, J. A., Fisher, V. A., Wynne, R. H., & Lenters, J. D. (1998). Global patterns of lake ice phenology and climate: Model simulations and observations. *Journal of Geophysical Research*, *103*(D22), 28627–29106. https://doi.org/10.1029/98JD02275

Wang, J., Song, C., Reager, J. T., Yao, F., Famiglietti, J. S., Sheng, Y., et al. (2018). Recent global decline in endorheic basin water storages. *Nature Geoscience*, *11*(12), 926–932. https://doi.org/10.1038/s41561-018-0265-7

Wang, S., Xu, C., Zhang, W., Chen, H., & Zhang, B. (2022). Human-Induced water loss from closed inland Lakes: Hydrological simulations in China's Daihai lake. *Journal of Hydrology*, *607*, 127552. https://doi.org/10.1016/j.jhydrol.2022.127552

Wang, W., Lee, X., Xiao, W., Liu, S., Schultz, N., Wang, Y., et al. (2018). Global lake evaporation accelerated by changes in surface energy allocation in a warmer climate. *Nature Geoscience*, *11*(6), 410–414. https://doi.org/10.1038/s41561-018-0114-8

Williams, G., Layman, K. L., & Stefan, H. G. (2004). Dependence of lake ice covers on climatic, geographic and bathymetric variables. *Cold Regions Science and Technology*, *40*(3), 145–164. https://doi.org/10.1016/j.coldregions.2004.06.010

Williams, S. G., & Stefan, H. G. (2006). Modeling of lake ice characteristics in North America using climate, geography, and lake bathymetry. *Journal of Cold Regions Engineering*, *20*(4), 140–167. https://doi.org/10.1061/(ASCE)0887-381X(2006)20:4(140)

Woolway, R. I., Kraemer, B. M., Lenters, J. D., Merchant, C. J., O'Reilly, C. M., & Sharma, S. (2020). Global lake responses to climate change. *Nature Reviews Earth and Environment*, *1*(8), 389–403. https://doi.org/10.1038/s43017-020-0067-5

Woolway, R. I., & Merchant, C. J. (2019). Worldwide alteration of lake mixing regimes in response to climate change. *Nature Geoscience*, *12*(4), 271–276. https://doi.org/10.1038/s41561-019-0322-x

Wu, R., Liu, Y., Zhang, S., Shi, X., Zhao, S., Lu, J., et al. (2023). Characterization of nitrogen and phosphorus at the ice-water-sediment interface and the effect of their migration on overlying water quality in Daihai Lake (China) during the freezing period. *Science of The Total Environment*, *893*, 164863. https://doi.org/10.1016/j.scitotenv.2023.164863

Wu, T. (2025). *Long-term variation in Lake Ice in a large endorheic Lake experiencing shrinkage in a semi-arid Region*. Mendeley Data, V2. https://doi.org/10.17632/j796j4ykfz.2

Wu, T., Qin, B., Zhu, G., Huttula, T., Lindfors, A., Ventelä, A. M., et al. (2018). The contribution of wind wave changes on diminishing ice period in Lake Pyhäjärvi during the last half-century. *Environmental Science and Pollution Research*, *25*, 24895–24906. https://doi.org/10.1007/s11356-018-2552-7

Wu, Y., Huang, A., Lu, Y., Fujisaki-Manome, A., Zhang, Z., Dai, X., & Wang, Y. (2023). Application of a three-dimensional coupled hydrodynamic-ice model to assess spatiotemporal variations in ice cover and underlying mechanisms in Lake Nam Co, Tibetan Plateau, 2007–2017. *Journal of Geophysical Research: Atmospheres*, *128*(24), e2023JD038844. https://doi.org/10.1029/2023JD038844

Xu, Y., Long, D., Li, X., Wang, Y., Zhao, F., & Cui, Y. (2024). Unveiling lake ice phenology in Central Asia under climate change with MODIS data and a two-step classification approach. *Remote Sensing of Environment*, *301*, 113955. https://doi.org/10.1016/j.rse.2023.113955

Yang, K., Hou, J., Wang, J., Lei, Y., Zhu, L., Chen, Y., et al. (2021). A new finding on the prevalence of rapid water warming during lake ice melting on the Tibetan Plateau. *Science Bulletin*, *66*(23), 2358–2361. https://doi.org/10.1016/j.scib.2021.07.022

Yang, T., Wu, T., Ji, X., Qin, B., Luan, C., Hu, R., & He, X. (2022). Reconstruction of the depletion process of lake water resources in semi-arid area under strong human activities-Taking Lake Daihai as an example. *Journal of Lake Sciences*, *34*(6), 2105–2121. (In Chinese with English abstract). https://doi.org/10.18307/2022.0623

Yang, W., Zhen, Y., Yao, Z., Yin, Q., Huang, X., & Li, W. (2023). Characterization for nitrogen metabolism of sediments in highland saline lake. *China Environmental Science*, *43*(3), 1328–1339. (In Chinese with English abstract). https://doi.org/10.19674/j.cnki.issn1000-6923.20221009.010

Yang, X., Yu, R., Sun, H., Li, X., & Wang, X. (2024). Greenhouse gas emissions from Boreal Lakes: Highlighting the impact of salinity and freezing period on emission dynamics. *Science of the Total Environment*, *955*, 177163. https://doi.org/10.1016/j.scitotenv.2024.177163

Ye, X., Anderson, E. J., Chu, P. Y., Huang, C., & Xue, P. (2019). Impact of water mixing and ice formation on the warming of Lake Superior: A model-guided mechanism study. *Limnology & Oceanography*, *64*(2), 558–574. https://doi.org/10.1002/lno.11059

Zhang, Z. (2020). *Study on the relationship between groundwater and surface water in Daihai Basin*. Hebei GEO University. https://doi.org/10.27752/d.cnki.gsjzj.2020.000301

Zhao, Q., Sun, J., & Zhu, G. (2012). Simulation and exploration of the mechanisms underlying the spatiotemporal distribution of surface mixed layer depth in a large shallow lake. *Advances in Atmospheric Sciences*, *29*(6), 1360–1373. https://doi.org/10.1007/s00376-012-1262-1